X-552-68-105

INTERCOMPARISON OF THE MINITRACK AND OPTICAL TRACKING NETWORKS USING GEOS-I LONG ARC ORBITAL SOLUTIONS

PART I

J. G. Marsh
C. E. Doll
Mission Trajectory Determination Branch
Mission and Trajectory Analysis Division
Tracking and Data Systems Directorate

R. J. Sandifer
W. A. Taylor
Wolf Research and Development Corporation
Applied Sciences Department
College Park, Maryland

December 1967

GODDARD SPACE FLIGHT CENTER
Greenbelt, Maryland

ABSTRACT

STADAN Minitrack network data are analyzed using an optically determined "standard orbit" of 5-1/4 days in length as a reference orbit. The "standard orbit" has an R.M.S. fit of 3".0. It is shown that this is adequate for evaluating Minitrack data. The "standard orbit" is based primarily upon GEOS-I flashing lamp sequence observations recorded by STADAN and SPEOPT MOTS 24" and 40", SAO Baker-Nunn, and USAF PC-1000 camera data.

A technique is devised to uncouple the refraction dependent from the refraction independent effects in the Minitrack residuals. The mean value of the refraction dependent residuals exhibited a shift of -0.2×10^{-3} in the region of 10°—30° elevation. The shift is insignificant at higher elevations. The mean value of the refraction independent residuals is approximately 0.02×10^{-3} with a standard deviation of 0.2×10^{-3}. This small mean value indicates that the Minitrack system when viewed as a whole appears relatively free of any strong bias. The Minitrack data were not included in the reference orbital solution. Analysis of the residuals by individual stations indicates that there may be some station dependent systematic errors present. Since these systematic errors were not removed by the usual calibration procedures, it is suggested that the use of an optically determined "standard orbit" would be a preferable method of calibrating individual Minitrack antenna arrays.

A Minitrack orbit for the same time period as the optical orbit was obtained with an R.M.S. fit of 0.19×10^{-3}. The Minitrack data used in this particular solution were not corrected for ionospheric or tropospheric refraction and were not weighted for elevation effects. Data down to 15° elevation were used in the solution. Positions differences between the Minitrack and Optical orbits produced an R.M.S. deviation of approximately 165 meters. This low figure is due in part to the use of an accurate gravity model and station positions consistent with this gravity model.

CONTENTS

APPENDIX

LIST OF ILLUSTRATIONS

APPENDIX ILLUSTRATIONS

LIST OF TABLES

APPENDIX TABLES

ABBREVIATIONS USED IN THE DOCUMENT

STADAN	Satellite Tracking and Data Acquisition Network
SAO	Smithsonian Astrophysical Observatory
MOTS	Minitrack Optical Tracking System
SPEOPT	Special Optical Tracking System (Same cameras used by MOTS)

TRACKING STATION CODE NAMES

A detailed description of the names, general locations and specific coordinates of the tracking stations corresponding to the adopted 6 character station code names used in the various tables and figures of this document is given in Appendix D.

INTERCOMPARISON OF THE MINITRACK AND OPTICAL TRACKING NETWORKS USING GEOS-I LONG ARC ORBITAL SOLUTIONS

1.0 INTRODUCTION

The primary objectives of the GEOS-I project are to utilize observations of GEOS-I for the purpose of connecting geodetic datums and defining the Earth's gravitational field to a specified degree of accuracy, improving positional accuracies of satellite tracking sites, and evaluation and calibration of tracking equipment (Reference 1, p. 1, 6). This report is concerned with the latter aspect of evaluation and calibration as applied to the Minitrack system.

One particular phase of the Minitrack—optical data intercomparison is presented in this report. GEOS-I long arc orbital solutions determined by optical observations only are used as a "standard orbit." The Minitrack residuals used in this analysis are calculated on the basis of this optically determined "standard orbit." As a result, the Minitrack residuals are calculated on the basis of an adjusted orbit which is not influenced by the Minitrack data set itself. Assuming that there are no significant systematic differences between the two data types, or perhaps equally important, no significant systematic differences between the tracking networks which recorded the two data types, this type of intercomparison can provide a useful tool for analyzing and evaluating the Minitrack data and network. It will be shown in a later section that the geometry of the reception pattern of the Minitrack Antenna arrays provides a possible method of uncoupling refraction dependent effects from refraction independent effects contained in the Minitrack residuals. In order to analyze the data from this point of view, the Minitrack residuals have been calculated from data which have not been pre-processed. As a result, the full effect of both tropospheric and ionospheric refraction are included in the residuals. By analyzing the data in this manner, it may be possible to determine how successful the uncoupling process can be performed. If the process is successful, then there is the added advantage that the data do not contain erroneous refraction effects which may arise from over-correcting or under-correcting the data for refraction. This problem is particularly sensitive because of the large uncertainties contained in knowledge of the state of the ionosphere. A later report (Part II) will analyze the Minitrack residuals with known refraction effects removed from the data. The analysis in the present report will be restricted to Minitrack data with all refraction effects included.

Section 9 of this report presents an intercomparison of two 5-1/4 day trajectories. One trajectory was computed on the basis of initial conditions adjusted by optical data only. The second trajectory was computed on the basis of initial conditions adjusted by Minitrack data only.

Using the optically determined orbit as the standard, the errors in position as determined by the Minitrack data had a standard deviation of approximately 165 meters. The Minitrack solution utilized data down to approximately 15° elevation. These data were not corrected for tropospheric or ionospheric refraction, and were not weighted to compensate for any deterioration of the data at the lower elevations. The reduction of the standard deviation to the relative low value of 165 meters may be attributed in part to the use of a sophisticated gravity model (SAO M-1 model—Reference 4) and the transformation of all tracking site locations to a datum (SAO C-5—Reference 4) utilizing the center of mass of the Earth as its origin and consistent with the gravity model used.

2.0 FEASIBILITY OF USING OPTICALLY DETERMINED "STANDARD ORBITS" TO EVALUATE AND CALIBRATE MINITRACK DATA

The feasibility of using optical observations of artificial satellites for calibration purposes has been previously noted by V. R. Simas (Reference 2, Sections 3.4.4, 3.4.5, p. 54). The large volume of high precision optical observations of GEOS-I currently available offers the first opportunity to analyze in depth the data obtained from the Minitrack network of the same satellite and to explore the feasibility of utilizing such optical data for calibration purposes. As noted in Appendix A, the upper precision limit obtainable at the most basic level of the electronics of the Minitrack system (the phase measurement level) is about 0.36 electrical degrees. This is equivalent to a precision of approximately 5" in terms of ability to measure angular arc in space under optimum conditions at the zenith. A more realistic figure for the overall expected precision of the Minitrack system at the equipment level is probably around 20" in terms of angular direction in space (Kaula, Reference 3, p. 84). The precision of the SAO optical observations is estimated to be approximately 2" (Reference 4, p. 43) for a single observation. Observations from the MOTS, PC-1000 and other cameras used in the GEOS-I program have an inherent precision which is slightly higher than the SAO figure. Whether or not this inherently greater accuracy is actually realized in practice will depend to a great extent upon the care which is exercised in reducing and preprocessing the data. Utilizing the SAO figure of 2" as an approximate gauge of the overall accuracy of an individual optical observation, there is sufficient justification in using optical observations as a standard to be used in analyzing and evaluating Minitrack network data provided that there exists no significant systematic differences between the two data types. This will be shown to be the case in a later section when considering the Minitrack network as a whole although there appear to exist systematic problems at individual Minitrack sites. Even if there exist significant systematic differences between the two data types, there still exists a strong justification for using optical data as a "standard" since all detectable error sources in this data type such as exist in star catalogues, plate measuring equipment, optical refraction, etc., have had the advantage of decades of thorough study by competent investigators, and the error limits of these sources are well known.

A certain amount of caution should be exercised when considering the MOTS optical observations as used in the "standard orbit" since the MOTS cameras are also used for calibrating the Minitrack system and any undetected systematic errors in the MOTS instrumentation will probably be propagated into the Minitrack calibration coefficients. However, since the MOTS cameras are

co-located with the center of the Minitrack antenna fine beam array, these optical observations may prove useful in verifying suspected systematic errors which have been detected by the Minitrack residuals.

One particularly useful conclusion of the current investigation is that an optically determined "standard orbit" has great value in detecting systematic errors at individual Minitrack sites. If these individual systematic errors can be identified and removed, the overall result will be a corresponding reduction in the R.M.S. of fit of orbits as determined by Minitrack data only. It is suggested also that the use of an optically determined "standard orbit" would be a preferable method of calibrating the individual Minitrack sites. The current method of calibration by means of simultaneously photographing an airborne flashing light with the MOTS cameras and detecting the 136.5 MC radio signal with the Minitrack antenna arrays, is not capable of detecting all systematic errors. Some obvious examples are errors in site location and timing errors. At best, the present calibration method can account only for local systematic errors.

3.0 SUMMARY OF OPTICAL DATA USED IN THE "STANDARD ORBIT" SOLUTION

The GEOS-I optical and Minitrack data used in the analysis described in this report were obtained from the NASA Space Science Data Center located at the Goddard Space Flight Center.

The "standard orbit" used in the calculation of the Minitrack residuals in the current analysis was determined completely from optical observations of GEOS-I. Minitrack observations were not used to adjust the standard orbit which was used as a basis for the calculation and subsequent analysis of the Minitrack residuals.

For the purpose of calibrating electronic equipment, the "active" GEOS-I optical data are particularly useful as a high precision data set. In addition to the reasons noted in Section 1, other factors contributing to this precision are the following:

1. The use of a stable on-board clock to trigger the optical beacon flash sequences permits the determination of the time of observation to millisecond accuracy.
2. The short duration (approximately 1.3 milliseconds) of the optical beacon flash sequences permitted the tracking cameras to record the observations as point images rather than as a streak against a background of reference stars thus enabling the right ascensions and declinations of the flashes to be determined to higher precision than normally obtained.

In general, the reduction methods associated with using reference stars as a means of determining angular position are the most accurate available of all current tracking systems.

The epoch of the standard orbit was $01^{H}\ 38^{M}\ 22\overset{S}{.}000$ 12/31/1965 UTC. The epoch was chosen at the beginning of the selected optical data set which extended to $06^{H}\ 45^{M}$ 1/5/1966 UTC, a total arc length of approximately 5-1/4 days covering 63 orbital revolutions of the spacecraft. The resulting R.M.S. of fit of this particular standard orbit was 3."0 based upon 1059 observations summarized in Table 3.1. A more detailed description of the names, general locations and specific

Table 3.1

Summary of GEOS-I Optical Observations Used in the Orbital Solution
for the Period $1^H\ 38^M$ 12/31/65 or $6^H\ 45^M$ 1/5/66.
(63 Orbital Revolutions)

Network	Station	Camera Type	No. of Observations				
			α	δ	α and δ	Type	No. Passes/ No. Flash Seq.
SAO	1ORGAN	Baker-Nunn	1	1	2	Passive	1/
	1MAUIO	Baker-Nunn	1	1	2	Passive	1/
	1NATOL	Baker-Nunn	4	4	8	Passive	4/
	OSLONR	Baker-Nunn	2	2	4	Passive	2/
	AUSBAK	Baker-Nunn	2	2	4	Passive	2/
	1SHRAZ	Baker-Nunn	1	1	2	Passive	1/
	1SPAIN	Baker-Nunn	3	3	6	Passive	3/
	1TOKYO	Baker-Nunn	6	6	12	Passive	6/
	1VILDO	Baker-Nunn	1	1	2	Passive	1/
	1JUPTR	Baker-Nunn	14	14	28	Active	1/2
	AGASSI	K-50	5	5	10	Active	1/1
	TOTAL		40 + 40 = 80 (21 + 21 = 42 total passive)				
SPEOPT	1COLBA	MOTS 40"	81	83	164	Active	8/13
	1JUM40	MOTS 40"	7	15	22	Active	3/3
	1BERMD	MOTS 40"	39	45	84	Active	5/7
	1PURIO	MOTS 40"	7	7	14	Active	1/1
	1DENVR	MOTS 40"	28	42	70	Active	4/6
	1JUM24	MOTS 40"	10	16	26	Active	3/3
	TOTAL		172 + 208 = 380			Active	
STADAN	1FTMYR	MOTS 40"	41	41	82	Active	4/6
	1BPOIN	MOTS 40"	23	30	53	Active	5/6
	1GFORK	MOTS 40"	11	15	26	Active	3/3
	1MOJAV	MOTS 40"	12	13	25	Active	2/2
	TOTAL		87 + 99 = 186				
USAF	HUNTER	PC-1000	30	29	59	Active	5/5
	SWANIS	PC-1000	7	7	14	Active	1/1
	GRDTRK	PC-1000	0	7	7	Active	1/1
	ANTIGA	PC-1000	13	13	26	Active	2/2
	SEMMES	PC-1000	30	30	60	Active	4/5
	CURACO	PC-1000	20	20	40	Active	3/3
	HOMEST	PC-1000	47	47	94	Active	4/6
	JUPRAF	PC-1000	12	5	17	Active	2/2
	BEDFRD	PC-1000	11	11	22	Active	2/2
	ABERDN	PC-1000	37	37	74	Active	6/6
	TOTAL		207 + 206 = 413				21/ Passive 70/86 Active

TOTAL OF ALL OBSERVATIONS = 1059
TOTAL PASSIVE OBSERVATIONS = 42

91 Total Station-Passes

coordinates of the tracking stations corresponding to the adopted 6 character station code names listed in this Table and other tables and figures of this report is given in Appendix D. The position and velocity vectors for the epoch $01^H\ 38^M\ 22^S.000$ 12/31/1965 UTC which were adjusted on the basis of the 1059 optical observations are given in Table 3.2. A summary of optical data coverage by time is shown in Figure 3.1

Table 3.2

Final Adjusted Position and Velocity Vectors at Epoch for the Optical "Standard Reference Orbit."

Optically Adjusted Position Vector	Optically Adjusted Velocity Vector
X: +5,690,537.7 meters	$\dot{X}$: -4,685.6198 meters/sec.
Y: +1,474,538.5 meters	$\dot{Y}$: +3,849.4695 meters/sec.
Z: +6,013,442.9 meters	$\dot{Z}$: +2,939.1210 meters/sec.
Epoch:	$01^H\ 38^M\ 22^S.000$ 12/31/1965 UTC
No. of Observations:	1059
Arc Length:	5-1/4 days
R.M.S. of Fit:	3".12

For comparable arc lengths, this R.M.S. of fit was not of the highest quality. A more typical figure for GEOS-I for this arc length would be approximately 2".0. However, this particular arc had been used for intercomparison with other instrumentation types and it was felt that a multiple instrument intercomparison would prove useful. In addition, the 3".0 R.M.S. of fit still places the optical data set well within the precision limits required for a Minitrack intercomparison.

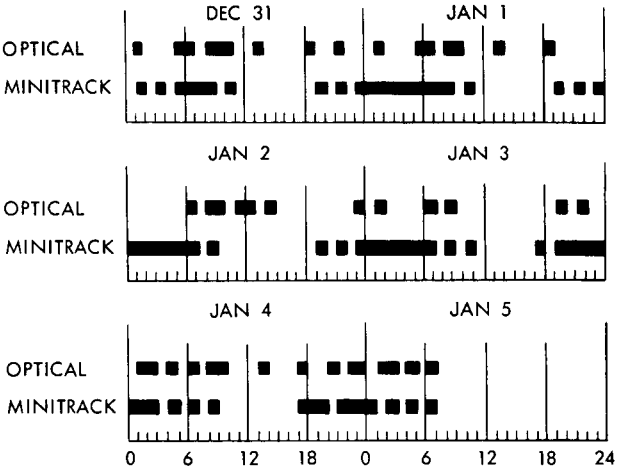

Figure 3.1—Summary of GEOS-I optical and Minitrack coverage for the period $1^H\ 38^M$ 12/31/65 to $6^H\ 45^M$ 1/5/66 UTC (63 orbital revolutions).

The 1059 optical observations are summarized in Table 3.1 by network, station, and type, i.e., whether the data were active or passive. In addition, a further breakdown is given of the active observations according to the number of passes over a particular station and the total number of flash sequences (maximum of 7 right ascensions and 7 declinations per flash sequence) per station. These data are more descriptive of the available station coverage and geometrical strength if they are described in terms of "station-passes."

The final tally reduces the total of 1059 optical observations to 86 active flash sequences during 70 "active station-passes" over the various optical stations and 21 "passive station-passes." The total number of "station-passes" was 91. The 21 "passive station-passes" were all obtained from the SAO network. Of the 70 "active station-passes," only 2 were obtained from the SAO network. The remaining 68 "active station-passes" were distributed as follows:

30 passes USAF Network PC-1000 cameras

24 passes SPEOPT Network MOTS 40" cameras

14 passes STADAN Network MOTS 40" cameras

The 68 passes from the Air Force, STADAN, and SPEOPT networks were all located on the North American Continent or its near vicinity (Figure 3.2). In addition, the only two "active station-passes" from SAO, at Agassiz, Massachusetts and Jupiter, Florida, are also on the North American Continent (Figure 3.3). At least one "passive station-pass" was obtained from every SAO station shown in Figure 3.3 except Olifantsfontein in South Africa. The R.M.S. of fit of 3."0 for the 5-1/4 days of optical observations was obtained using the SAO M-1 gravity model modified by the GEOS-I resonant harmonics ($C_{13,12}$, $C_{14,12}$, $C_{15,12}$, $S_{13,12}$, $S_{14,12}$, $S_{15,12}$) as redetermined by SAO (Appendix C; Reference 4, p. 2; Reference 5, p. 5). All tracking station locations were transformed to the SAO C-5 system (Reference 4, p. 2; Appendix D).

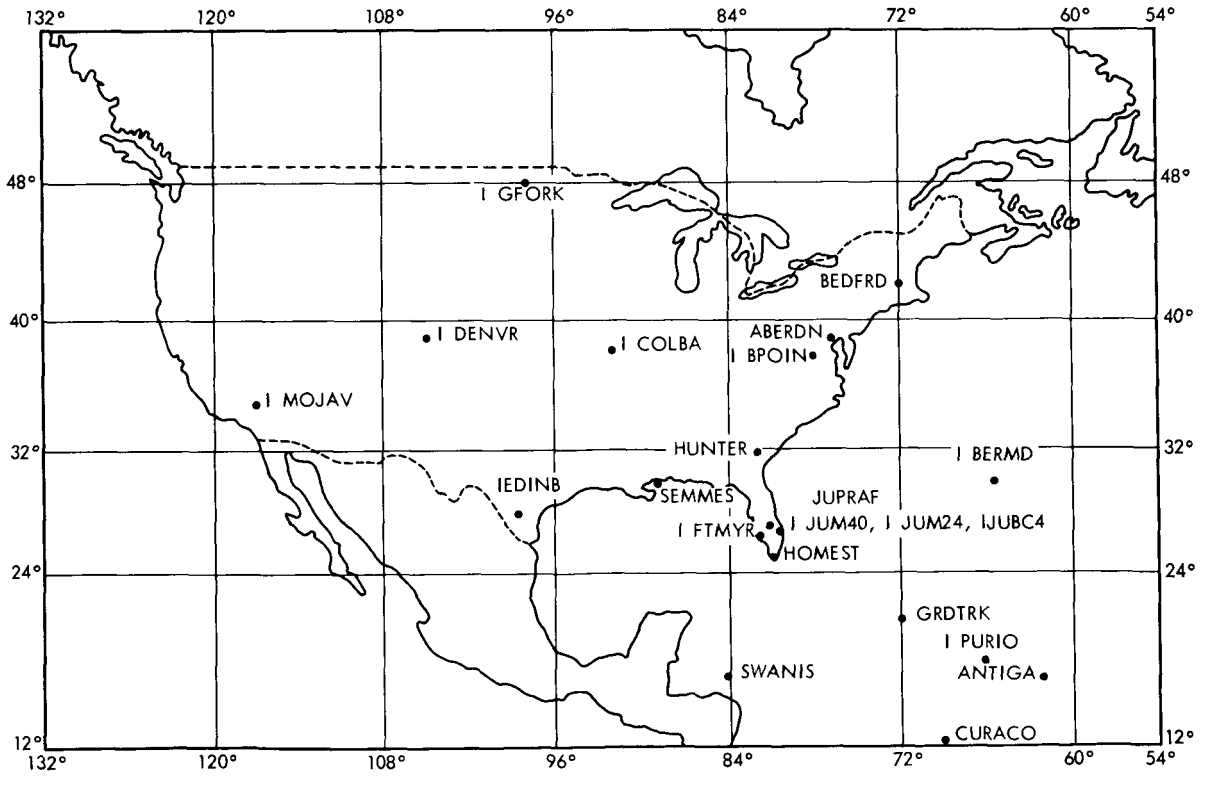

Figure 3.2—Location of STADAN, SPEOPT and USAF camera sites whose observations were used in the orbital solution.

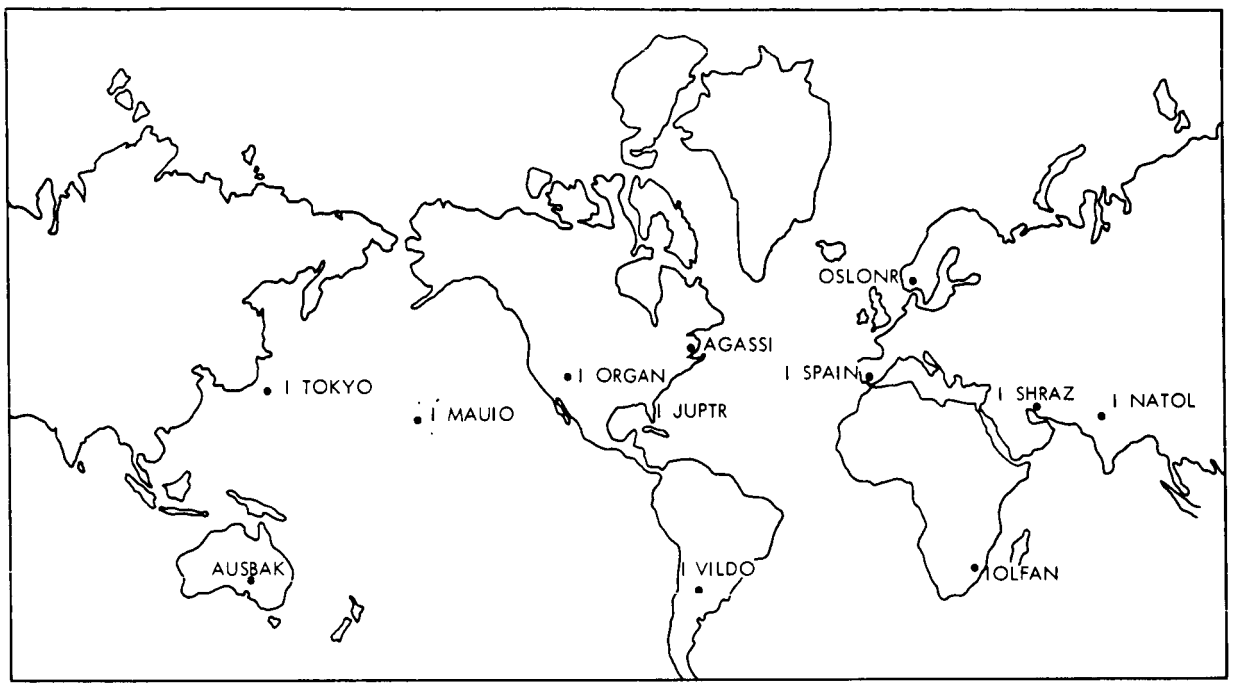

Figure 3.3—SAO Baker-Nunn camera site locations.

4.0 SUMMARY OF MINITRACK DATA AVAILABLE FROM THE SPACE SCIENCE DATA CENTER FOR THE PERIOD OF INTEREST AND DATA REJECTED BEFORE ANALYSIS

The Minitrack data as obtained from the NASA Space Science Data Center consist of 1 to 3 pairs of direction cosines per station-pass. These data in turn have been reduced by Goddard from approximately 30 pairs of phase difference measurements per pass as transmitted to Goddard from the various Minitrack stations. Goddard transforms these data to direction cosines and reduces them to approximately 1 to 3 data pairs of direction cosines by means of a polynomial smoothing process. This is the only data preprocessing performed before the data are transmitted to the Space Science Data Center or used by Goddard's own orbit differential correction program. The R.M.S. of fit of the polynomial smoothing process is slightly less than 0.1×10^{-3} on the average. (Reference 17)

During normal operations the Minitrack stations do not track below 20° zenith distance except during early launch phases. In the case of GEOS-I, an exception was made and tracking was performed almost to the horizon. For the current analysis, Minitrack observations are available down to 15° elevation so that there is a sufficient span of data in that dimension to investigate refraction effects.

The Minitrack data originally available for analysis from the Space Science Data Center for the period of interest consisted of 482 observations and is summarized by station in the first column of Table 4.1. After a rejection criterion described in the next paragraph was applied to the data, 436 data points remained for the analysis. These data are summarized in Table 4.3. The 436 data

Table 4.1

Summary of Minitrack Data Rejected for Analysis Purposes
for the Period $1^H\ 38^M$ 12/31/65 to $6^H\ 45^M$ 1/5/66.
(Approximately 63 Orbital Revolutions)

Station	ℓ				m			
	Total No. of Obs. Available	No. of Obs. with Residuals Greater Than 0.5×10^{-3}	Total No. of Obs. Rejected	% of Obs. with Residuals Greater Than 0.5×10^{-3}	Total No. of Obs. Available	No. of Obs. with Residuals Greater Than 0.5×10^{-3}	Total No. of Obs. Rejected	% of Obs. with Residuals Greater Than 0.5×10^{-3}
1. BPOINT	50	1	4	2.0	50	2	4	4.0
2. COLEGE	25	3	4	12.0	25	2	4	8.0
3. FTMYRS	21	2	4	9.5	21	3	4	14.3
4. GFORKS	29	2	2	6.9	29	1	2	3.4
5. JOBURG	2	0	0	0.0	2	0	0	0.0
6. LIMAPU	6	0	0	0.0	6	0	0	0.0
7. MOJAVE	38	1	2	2.6	38	1	2	2.6
8. NEWFLD	38	0	2	0.0	38	1	2	2.6
9. OOMERA	6	1	2	16.7	6	1	2	16.7
10. QUITOE	4	0	0	0.0	4	0	0	0.0
11. SNTAGO	4	0	0	0.0	4	0	0	0.0
12. WNKFLD	18	3	3	16.7	18	2	3	11.1
ℓ	241	13	23	5.4%	241	13	23	5.4%
m	241	13	23	5.4%				
TOTAL	482	26	46	5.4%				

5.4% of Data Exceeded 0.5×10^{-3}

points comprise 158 station-passes compared to 91 station-passes of optical data. For the Minitrack data also, the geometry is strongly oriented towards the North American continent with 29 passes at Blossom Point, Maryland, 26 passes at St. Johns, Newfoundland and 25 passes at Mojave, California. At least one observation pair was obtained from every Minitrack station (Figure 4.1) except the one located at Tananarive.

A cut-off criterion of 0.5×10^{-3} in direction cosine residuals was used in the rejection of data to be used in the analysis. This particular figure was chosen for convenience in the analysis of the residuals and to correspond to approximately 2-1/2 times the R.M.S. of the orbital fit. For data rejection purposes also, the "standard orbit" was used as the basis for calculating the Minitrack residuals.

Approximately 5% of all Minitrack data available from the NASA Space Science Data Center during the period of analysis exceeded this figure. Thus the percentage of data rejected on the basis of the 0.5×10^{-3} cutoff criterion is statistically consistent with the assumption of a normal distribution of the residuals (see residual plot in Figure 7.2). Minitrack data rejected on the basis of this criterion is summarized by station in Table 4.2. The magnitude of the residuals enclosed by a rectangle in this table were less than the criterion but were omitted from the analysis because their counterpart exceeded the criterion. One residual pair from Blossom Point, Maryland at 17°

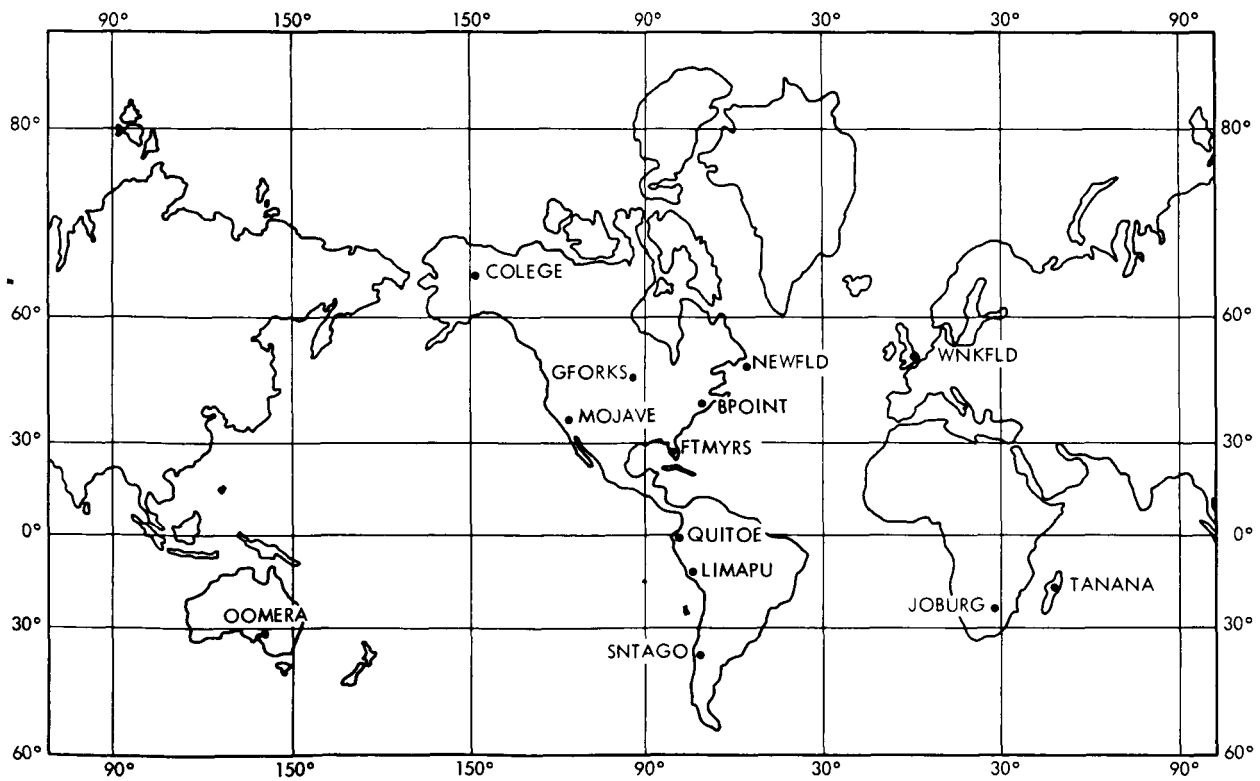

Figure 4.1—STADAN 136 MC Minitrack interferometer site locations.

Table 4.2

Table of Residuals of Minitrack Data Rejected for Analysis Purposes.
(Rejection criterion—0.5×10^{-3})

Station	$\Delta\ell$	Δm	Elevation
GFORKS	2.54×10^{-3}	1.74×10^{-3}	71°
	6.02×10^{-3}	$\boxed{.07} \times 10^{-3}$	44
BPOINT	507.12×10^{-3}	452.86×10^{-3}	-56
	$\boxed{.19} \times 10^{-3}$	$.61 \times 10^{-3}$	23
	$\boxed{.03} \times 10^{-3}$	$\boxed{.06} \times 10^{-3}$	17
	$\boxed{.29} \times 10^{-3}$	$.83 \times 10^{-3}$	21
COLEGE	18.15×10^{-3}	$\boxed{.30} \times 10^{-3}$	23
	17.97×10^{-3}	23.78×10^{-3}	20
	17.40×10^{-3}	17.56×10^{-3}	19
	$.51 \times 10^{-3}$	$\boxed{.15} \times 10^{-3}$	28
FTMYRS	$.74 \times 10^{-3}$	$\boxed{.09} \times 10^{-3}$	50
	$.61 \times 10^{-3}$	$.55 \times 10^{-3}$	23
	$\boxed{.27} \times 10^{-3}$	$.58 \times 10^{-3}$	28
	$\boxed{.41} \times 10^{-3}$	$.59 \times 10^{-3}$	27
MOJAVE	17.22×10^{-3}	$.06 \times 10^{-3}$	22
	$\boxed{.12} \times 10^{-3}$	$.54 \times 10^{-3}$	34
NEWFLD	$\boxed{.23} \times 10^{-3}$	$.52 \times 10^{-3}$	17
	$\boxed{.12} \times 10^{-3}$	$.61 \times 10^{-3}$	70
WNKFLD	132.50×10^{-3}	113.17×10^{-3}	70
	187.89×10^{-3}	47.89×10^{-3}	61
	1.99×10^{-3}	$\boxed{.14} \times 10^{-3}$	62
OOMERA	$.62 \times 10^{-3}$	$\boxed{.25} \times 10^{-3}$	47
	$\boxed{.38} \times 10^{-3}$	$.62 \times 10^{-3}$	63

Any residual enclosed by a rectangle is less than the rejection criterion but was omitted from the analysis because its counterpart exceeded the criterion. Although both BPOINT residuals at 17° elevation were less than the rejection criterion, they were erroneously rejected.

elevation was erroneously rejected due to a faulty computer printout on the first pass through the data. A final summary of the total number of original observations and number of observations rejected by station is shown in Table 4.3. The total number of observations rejected from the analysis was 46 of a total of 482 or 9-1/2% of the total data available. This is higher than the 5.4% of the data which actually exceeded the rejection criterion of 0.5×10^{-3} since both data points of a pair were rejected even though only 1 of the 2 points may have exceeded the criterion. The rejection of 16.7% of the data from Woomera, Australia is statistically insignificant because of the small number of observations available from that station (6 pairs). Of perhaps more significance is the 10% data rejection rate from College, Alaska. It will be shown later than there is a strong bias in the residuals from this station which may account for the high rejection rate.

Table 4.3

Summary of Minitrack Observations Used in Intercomparisons for the Period $1^H\ 38^M$ 12/31/65 to $6^H\ 45^M$ 1/5/66. (Approximately 63 Orbital Revolutions)

Station	No. of Observations			Location
	ℓ	m	No. of Passes	
1. BPOINT	46	46	29	Blossom Point, Maryland
2. COLEGE	21	21	18	College, Alaska
3. FTMYRS	17	17	12	Fort Myers, Florida
4. GFORKS	27	27	19	East Grand Forks, Minnesota
5. JOBURG	2	2	2	Johannesburg, South Africa
6. LIMAPU	6	6	4	Lima, Peru
7. MOJAVE	36	36	25	Mojave, California
8. NEWFLD	36	36	26	St. Johns, Newfoundland
9. OOMERA	4	4	4	Woomera, Australia
10. QUITOE	4	4	3	Quito, Ecuador
11. SNTAGO	4	4	4	Santiago, Chile
12. WNKFLD	15	15	12	Winkfield, England
TOTAL	218 + 218		158 Total Station-Passes = 436	

R.M.S. Orbital Fit Using Minitrack Data Only = 0.19×10^{-3}

All Minitrack Data Rejected Whose Residuals From Optically Determined Orbit Exceeded 0.5×10^{-3} (5% of Smoothed Data Available From Data Center)

An orbit is described in Section 9 of this report which is adjusted on the basis of Minitrack data only. These data were not corrected for tropospheric or ionospheric refraction effects and were not weighted in the orbital adjustment process. The resulting R.M.S. of fit was 0.19×10^{-3}. On the basis of this figure then, 5% of the Minitrack data available from the NASA Space Science Data Center exceeded this R.M.S. fit of the Minitrack determined orbit. It is significant that when the Minitrack residuals were recalculated on the basis of the same orbital arc as adjusted by Minitrack data only, there were no additional residuals encountered falling outside the 0.5×10^{-3} criterion originally used to reject Minitrack residuals calculated on the basis of the "standard orbit."

5.0 GEOMETRY OF THE MINITRACK "EQUATORIAL" AND "POLAR" MODES OF TRACKING

A more complete description of the 136 MC Minitrack Interferometer Tracking system and the resulting tracking geometry is described in Appendix A. The tracking geometry is summarized in Figure 5.1. There are two possible modes of tracking, the "equatorial" tracking mode and the "polar" tracking mode. In the equatorial mode, the "fine beam" is oriented in a North-South direction, with the long portion of the beam stretching 50° on each side of the zenith and 5° on each side of the zenith in the East-West direction relative to the station center C. When tracking in the polar tracking mode, the long portion of the "fine beam" is oriented East-West and the narrow portion oriented North-South. The particular mode of tracking is usually determined by the direction in which the satellite is approaching the station. It is possible to switch electronically from one mode to the other fairly quickly. Several passes of GEOS-I during the period of analysis were tracked in both modes during the same pass.

The observations available as data are the direction cosines ℓ and m which are equal respectively to the cosines of the angles α and β as indicated in Figure 5.1. A vector directed towards the satellite is indicated in this figure in both the equatorial and polar tracking modes. Observational data are usually available only when the satellite is located inside this fan-shaped "fine beam"

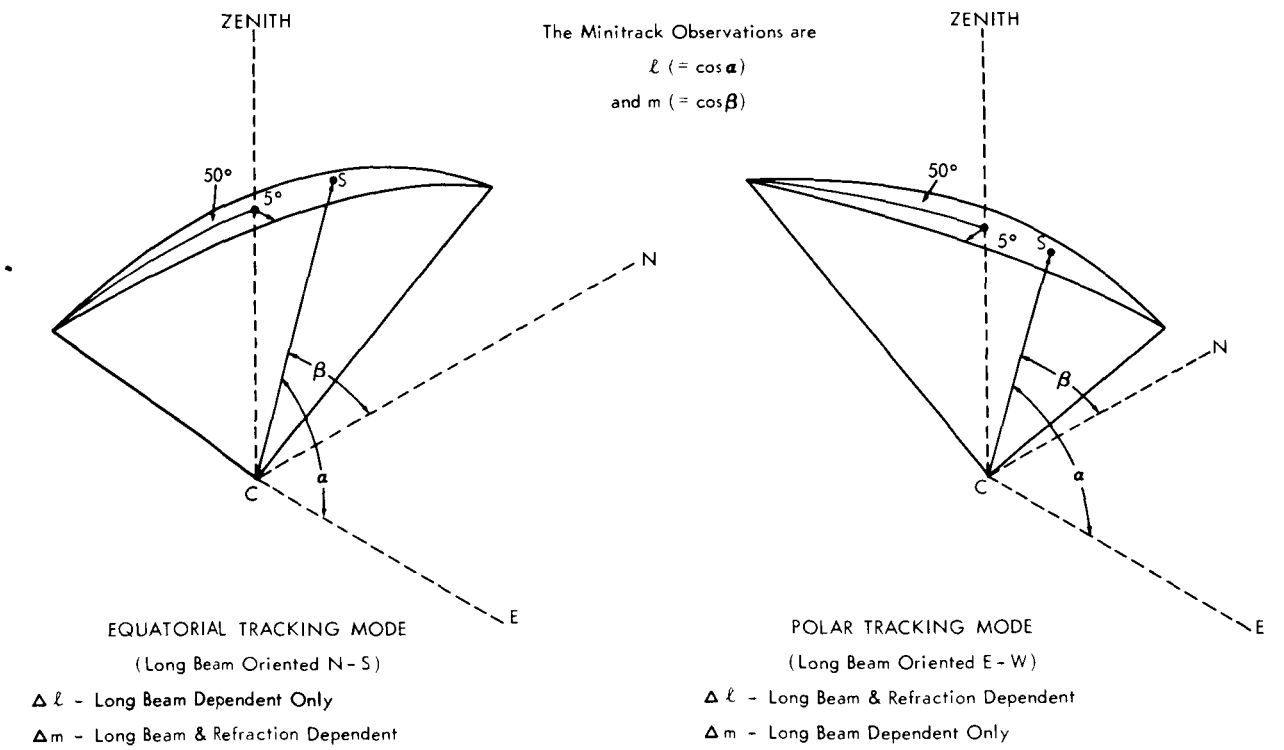

Figure 5.1—Approximate reception pattern of the fine beam of the 136 MC Minitrack antenna array in the equatorial and polar tracking modes.

although there are occasional data outside this pattern in the "side lobes." Observations made within the "fine beam" are considered to be more accurate than observations made in the side lobes.

The method of obtaining calibration coefficients for the individual Minitrack stations is described in References 6, 11, 15, and 18. The method employed by Goddard Space Flight Center in transforming the raw Minitrack phase measurements to direction cosines, making use of these calibration coefficients and other relevant information, is described in References 2, 7, 8, 9, 10, 17, 19, and 20a, b, and c. The corrections for ionospheric and tropospheric refraction as employed by the operational orbit determination program is described in References 21a, b, and 22.

Refraction corrections were not applied to the measurements used in the analysis of this report for the purpose indicated in the previous section.

The Minitrack antenna arrays are laid out by employing a method of leveling corresponding to the astronomical zenith. The raw phase measurements are referenced to an "electrical" zenith defined by the antenna system. However, the calibration equations referred to above transform the raw phase measurements to direction cosines relative to the geodetic zenith.

6.0 USE OF THE MINITRACK GEOMETRY TO UNCOUPLE REFRACTION DEPENDENT FROM REFRACTION INDEPENDENT EFFECTS IN THE MINITRACK RESIDUALS

By considering the geometry of the antenna pattern in Figure 5.1 more carefully, it is seen that in the equatorial tracking mode, the angle γ will never be less than 85° nor more than 95° and the angle β will be approximately equal to the elevation angle or its supplement. In the polar tracking mode, the situation is reversed and β will always be between 85° and 95° and γ will be approximately equal to the elevation angle or its supplement. For the purposes of the analysis in this report, it will be assumed on the basis of this configuration that any systematic errors due to refraction are not present in $\Delta\ell_{eq.}$ and Δm_{polar}, ($\Delta\ell_{eq.}$ = residuals in the ℓ direction cosine when tracking in the equatorial mode; Δm_{polar} = residuals in the m direction cosine when tracking in the polar tracking mode). Whatever systematic effects may be present in $\Delta\ell_{eq.}$ and Δm_{polar} will be called a "beam only" effect. It will be assumed that $\Delta\ell_{polar}$ and $\Delta m_{eq.}$, i.e., the residuals in the direction cosine ℓ when tracking in the polar tracking mode and in the direction cosine m when tracking in the equatorial tracking mode, will contain both systematic "beam only" effects and systematic "refraction" effects. Any systematic effects which may be due to position across the narrow part of the beam will be neglected.

7.0 CONSIDERATION OF RESIDUALS FROM THE MINITRACK NETWORK AS A WHOLE

The Minitrack residuals were calculated on the basis of the 5-1/4 day standard orbit described in Section 3. In order to determine the best method to use in detecting possible systematic trends, the residuals were analyzed by considering the various possible methods of combining $\Delta\ell$ and Δm. Histograms for the entire set of residuals from all 12 stations are shown in Figure 7.1, with $\Delta\ell$ and

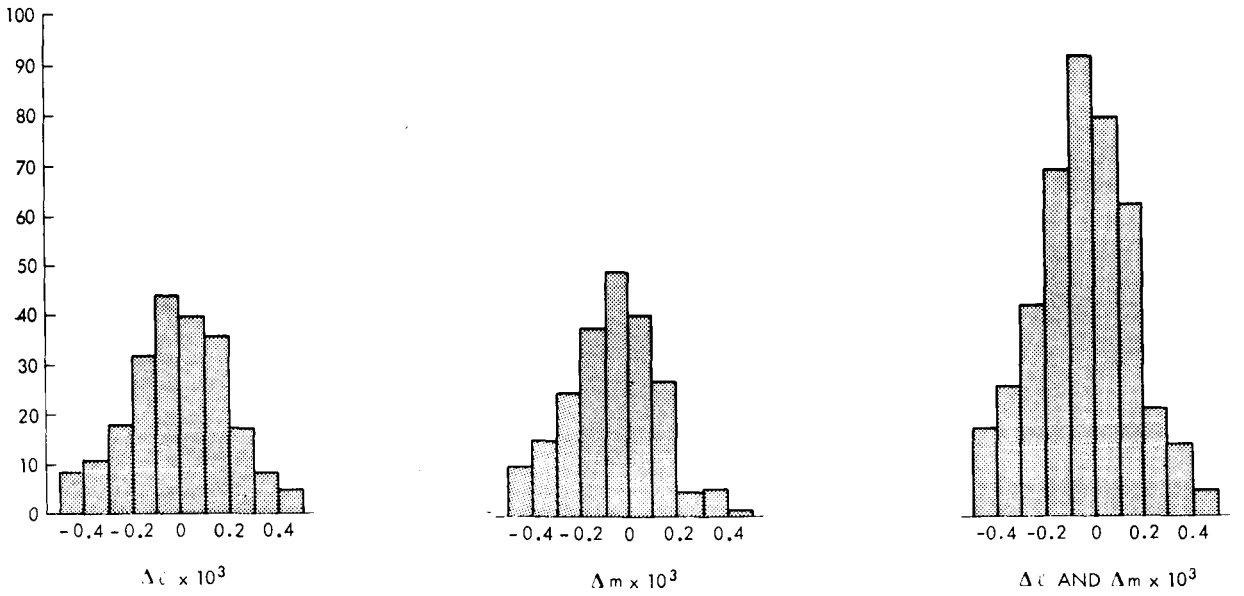

Figure 7.1—Histograms of Minitrack residuals calculated from optically determined "standard orbit"—summary from all stations.

Δm together and separately. There is no obvious evidence from these histograms to suggest any strong systematic differences between the optical data and the Minitrack data considered as a whole. No distinction has been made at this point concerning the Minitrack mode of tracking (i.e., equatorial or polar).

The residuals which were the basis of the histograms depicted in Figure 7.1 were then grouped according to the mode of tracking. These results are displayed in the form of 3 dimensional histograms in Figure 7.2 showing relative frequency as a function of both magnitude of the residual in steps of 0.1×10^{-3} and by elevation angle in steps of 20°. The histogram labeled "Beam Only Effect" is obtained from the frequency of $\Delta\ell_{eq.}$ and Δm_{polar}. The histogram labeled "Beam Only + Refraction Effects" is obtained from the frequency of $\Delta\ell_{polar}$ and $\Delta m_{eq.}$ residuals. The mean value and standard deviations of the residuals in the elevation dimension are printed at the top. For the "Beam Only Effect" the mean values in the different elevation dimensions remain fairly close to 0. In the "Beam Only + Refraction Effects" histogram, there is a definite shift of the mean value of the residuals to the negative at low elevations. In the 10° to 30° elevation dimension, the shift amounts to -0.2×10^{-3} which is of the order of magnitude to be expected due to refraction effects only, and is in the correct direction. The small magnitude of the mean value of the "Beam Only Effects" set of residuals is further verification of no strong systematic differences between optical and Minitrack data sets. The relatively large values of the standard deviations can be explained on the basis of individual Minitrack station biases. This effect will be shown in the next section.

8.0 SYSTEMATIC ERRORS AT INDIVIDUAL MINITRACK SITES

In order to detect possible biases at individual Minitrack station sites, the residuals were replotted on a station basis. Figures 8.1a through 8.11 depict the residuals for each station separately.

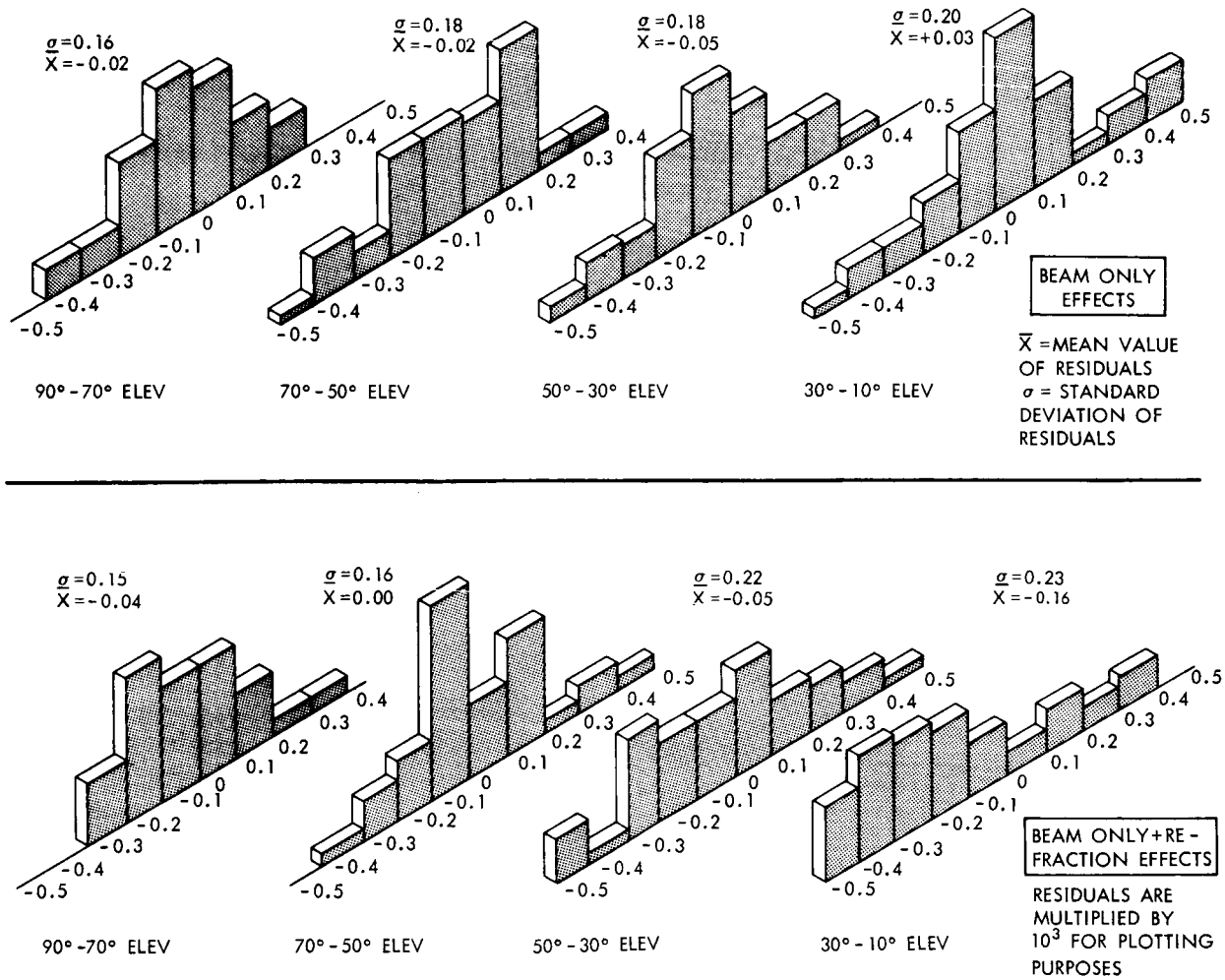

Figure 7.2—Histograms of Minitrack residuals separated into "beam only" and "beam only + refraction" effects in steps of 20° in elevation angle.

In these plots by individual station, the ℓ and m direction cosine residuals have been plotted separately as a function of elevation angle. A circle represents a residual obtained from an observation when the equipment was operating in the polar tracking mode. A dot represents a residual obtained from an observation when the equipment was operating in the equatorial mode. This same residual set has been summarized in histogram form in Figures 8.2a and 8.2b without regard to tracking mode. There are pronounced biases particularly at the stations of College, Alaska (COLEGE) and Mojave, California (MOJAVE). In particular, College has no positive residuals in $\Delta\ell$ and no negative residuals in Δm. At Mojave, there is strong positive bias in the $\Delta\ell$ residuals and a strong negative bias in the Δm residuals.

Considerable caution must be exercised in attempting to analyze residual sets which may or may not contain biases. Also a certain ingenuity is often required in order to unmask and identify these biases if they do exist. For example, the histograms in Figure 7.1 which summarize the frequency of the Minitrack residuals from all stations both collectively (i.e. $\Delta\ell$ and Δm together)

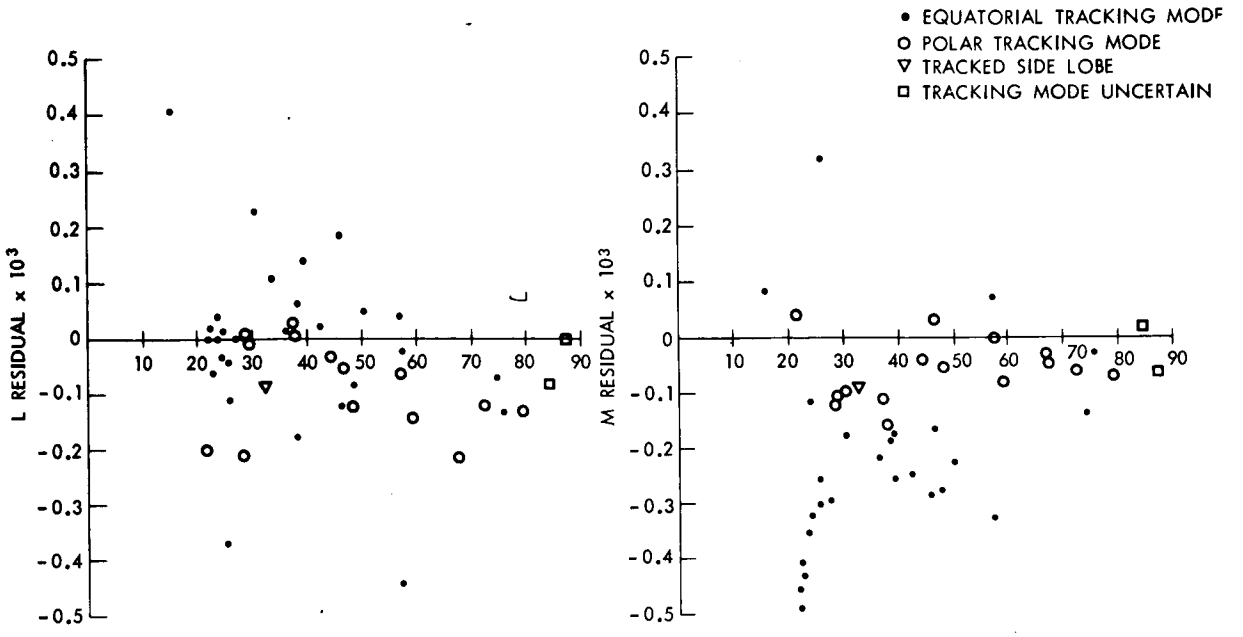

ELEVATION VS DIRECTION COSINE RESIDUAL x 10^3

a. Blossom Point, Maryland 46 observations

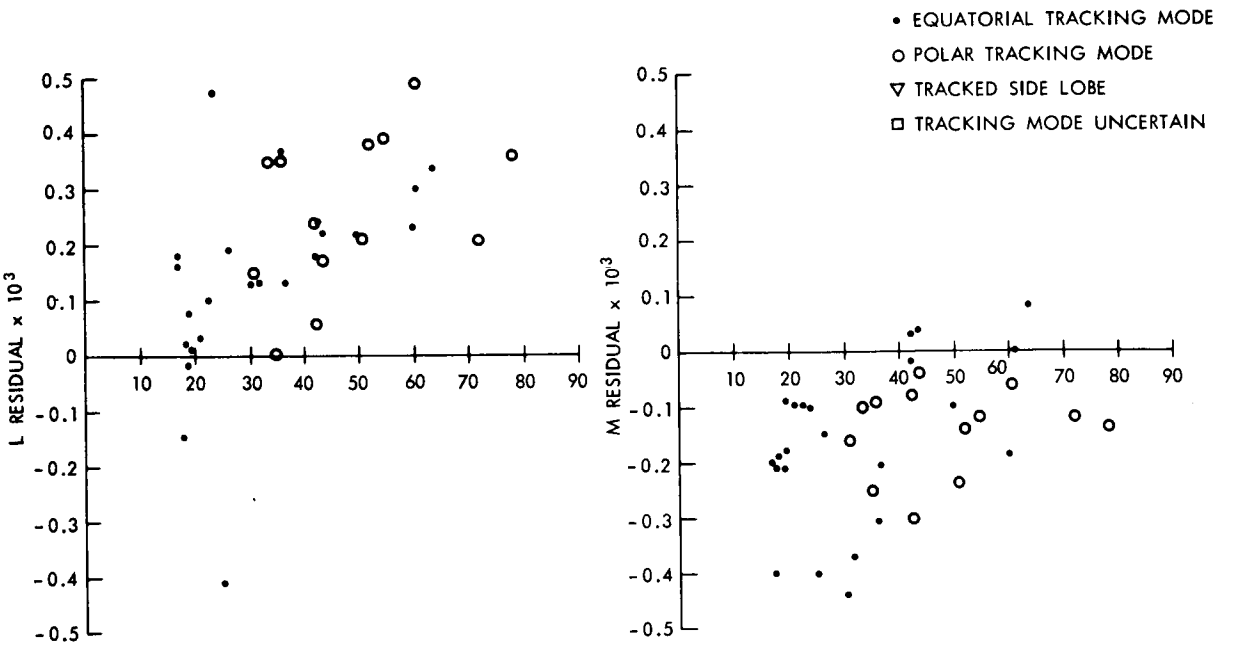

ELEVATION VS DIRECTION COSINE RESIDUAL x 10^3

b. Mojave, California 36 observations

Figure 8.1—Plots of elevation vs. direction cosine residuals (elevation vs. $\Delta l \times 10^3$ and elevation vs. $\Delta m \times 10^3$) and mode of tracking (polar or equatorial).

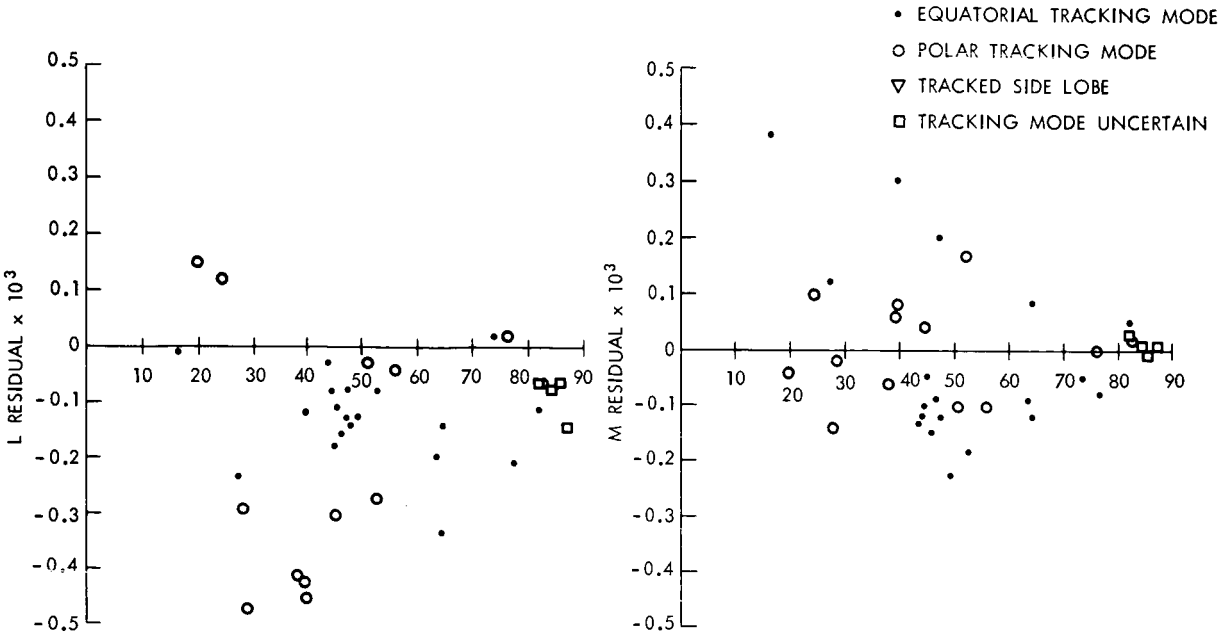

ELEVATION VS DIRECTION COSINE RESIDUAL x 10^3

c. St. Johns, Newfoundland 36 observations

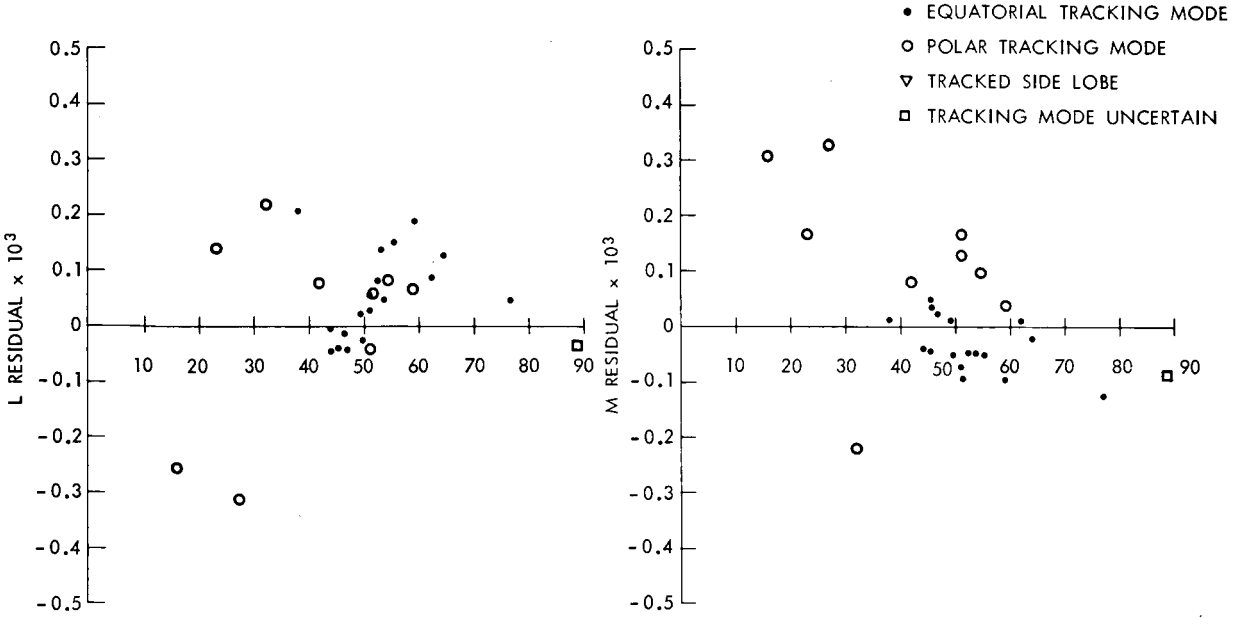

ELEVATION VS DIRECTION COSINE RESIDUAL x 10^3

d. East Grand Forks, Minnesota 27 observations

Figure 8.1—Plots of elevation vs. direction cosine residuals (elevation vs. $\Delta \ell$ x 10^3 and elevation vs. Δm x 10^3) and mode of tracking (polar or equatorial).

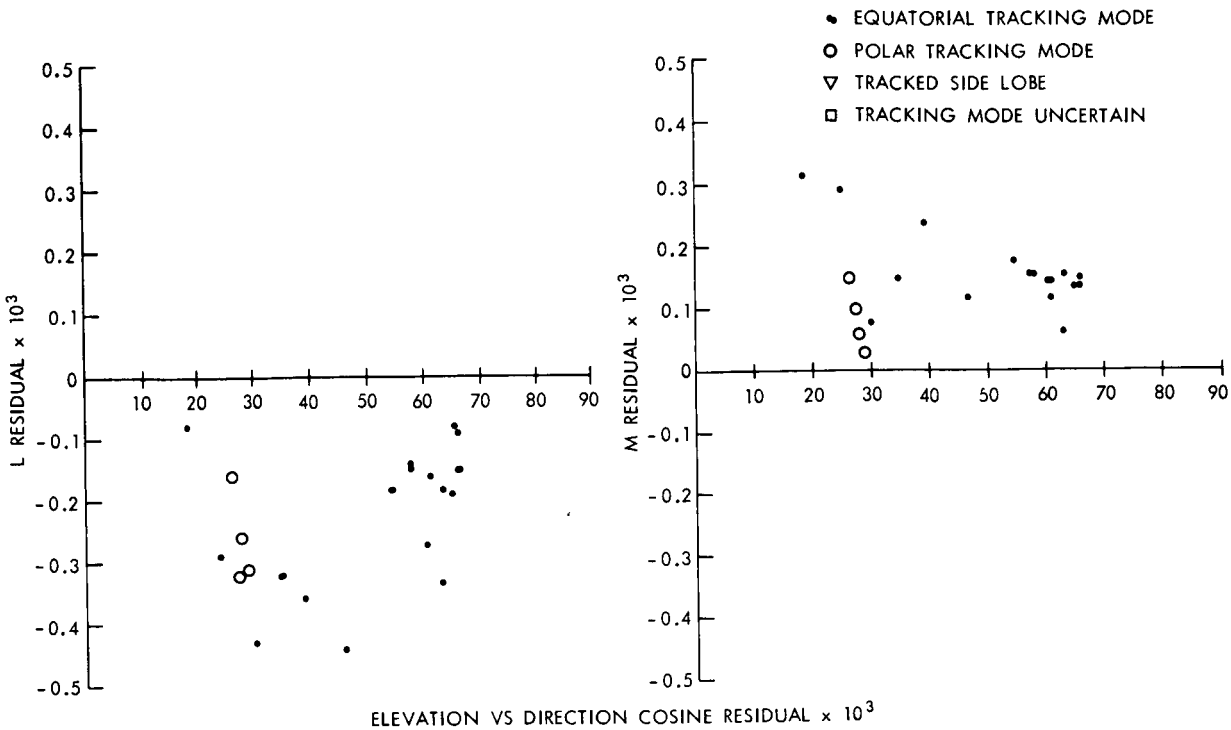

e. College, Alaska 21 observations

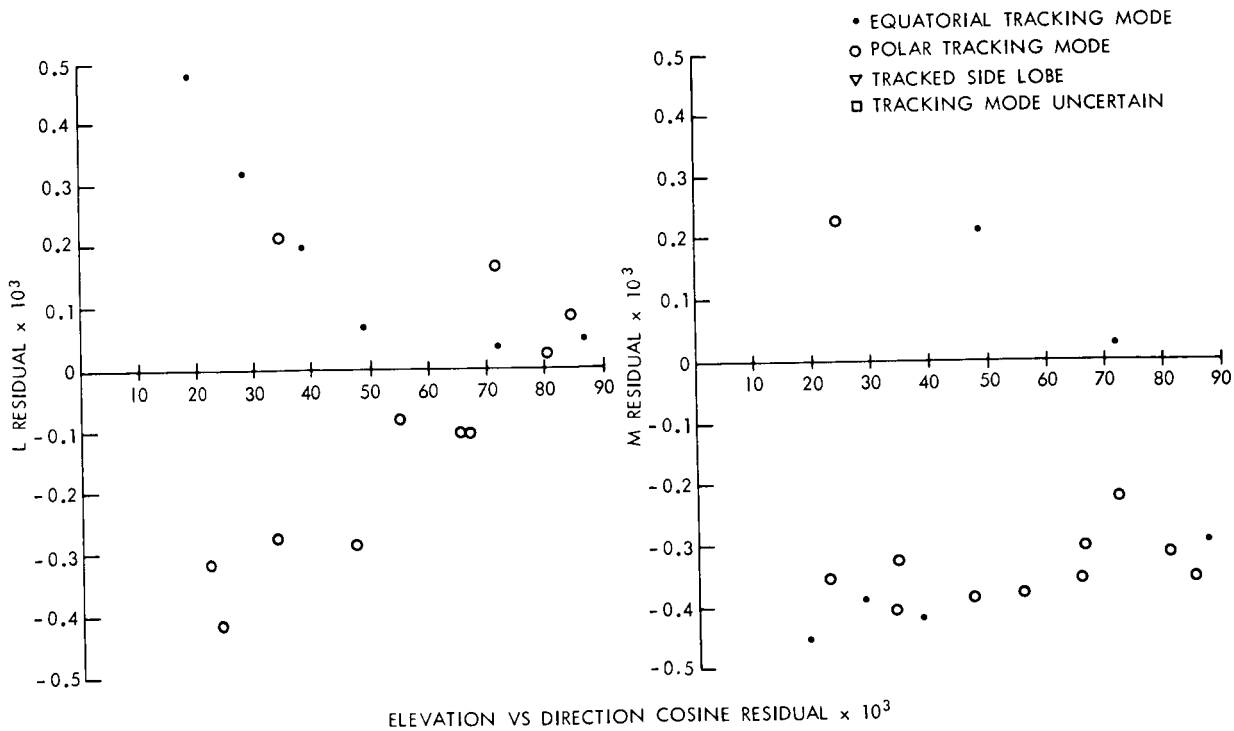

f. Fort Myers, Florida 17 observations

Figure 8.1—Plots of elevation vs. direction cosine residuals (elevation vs. $\Delta l \times 10^3$ and elevation vs. $\Delta m \times 10^3$) and mode of tracking (polar or equatorial).

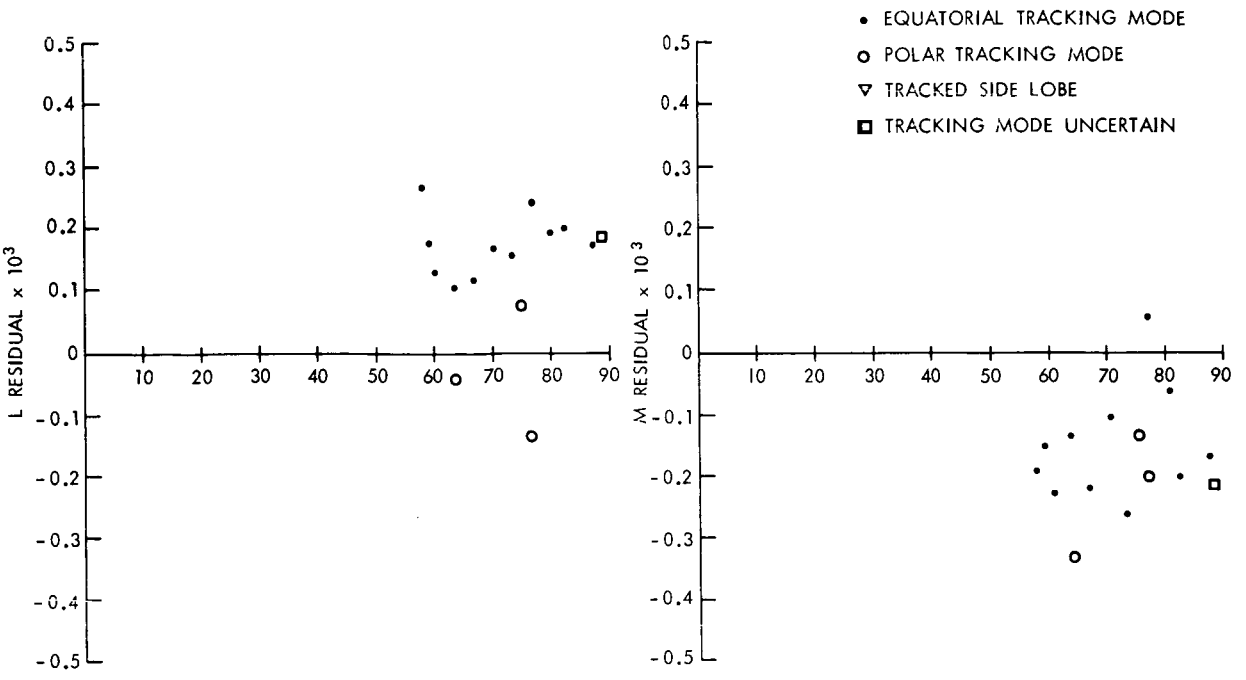

ELEVATION VS DIRECTION COSINE RESIDUAL x 10^3

g. Winkfield, England 15 observations

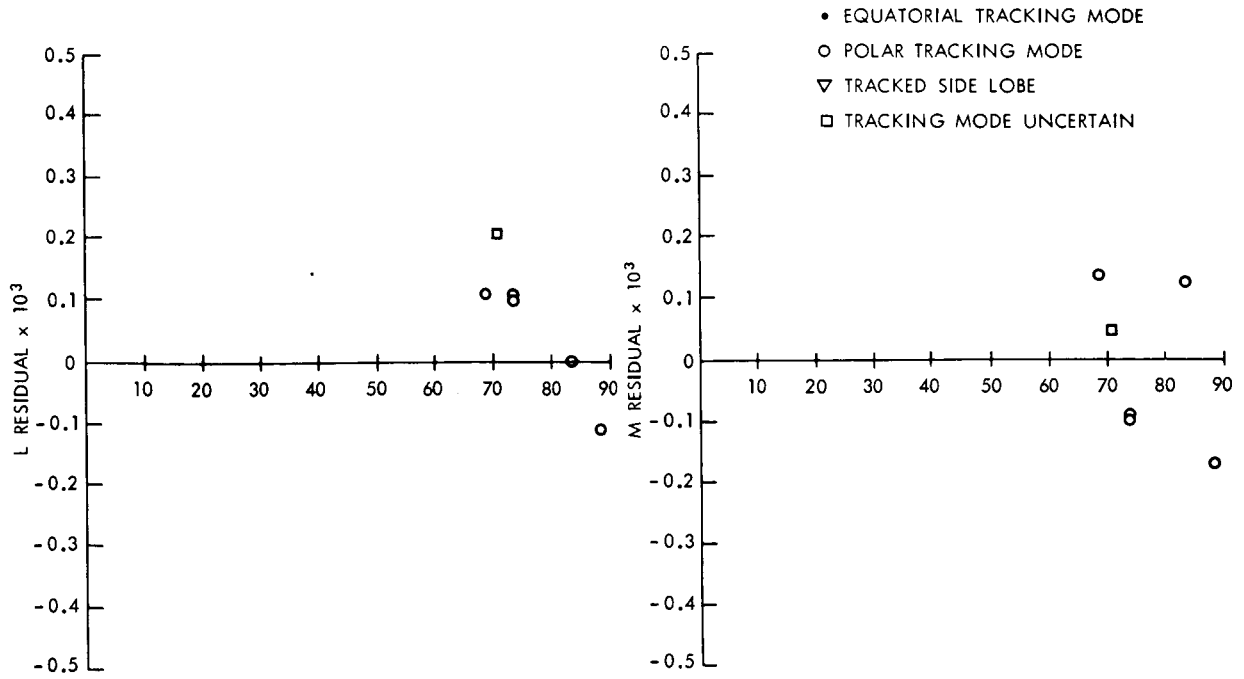

ELEVATION VS DIRECTION COSINE RESIDUAL x 10^3

h. Lima, Peru 6 observations

Figure 8.1—Plots of elevation vs. direction cosine residuals (elevation vs. Δf x 10^3 and elevation vs. Δm x 10^3) and mode of tracking (polar or equatorial).

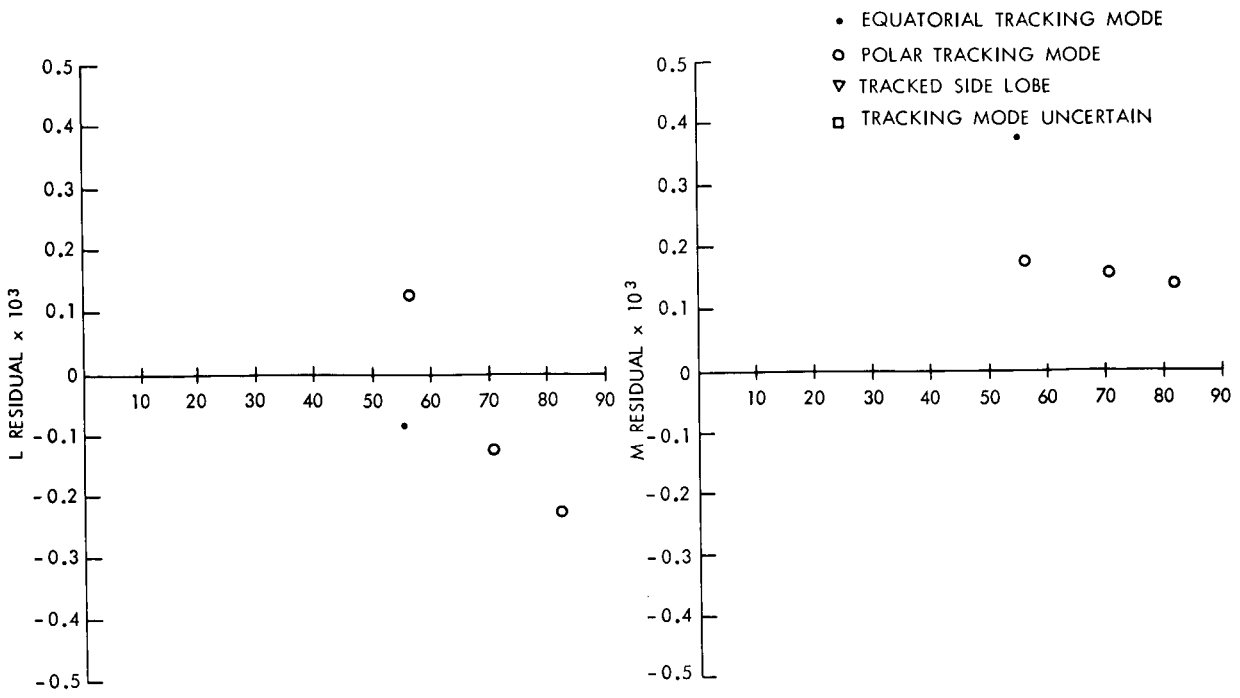

i. Quito, Ecuador 4 observations

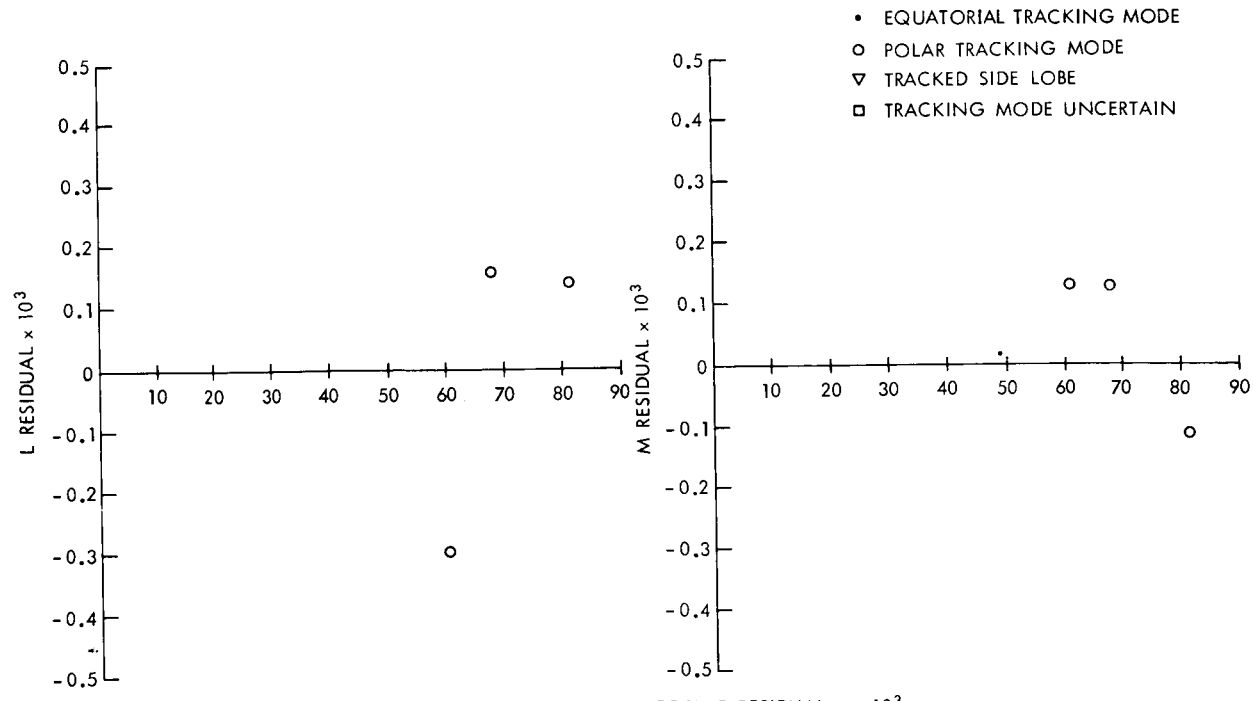

j. Santiago, Chile 4 observations

Figure 8.1—Plots of elevation vs. direction cosine residuals (elevation vs. $\Delta l \times 10^3$ and elevation vs. $\Delta m \times 10^3$) and mode of tracking (polar or equatorial).

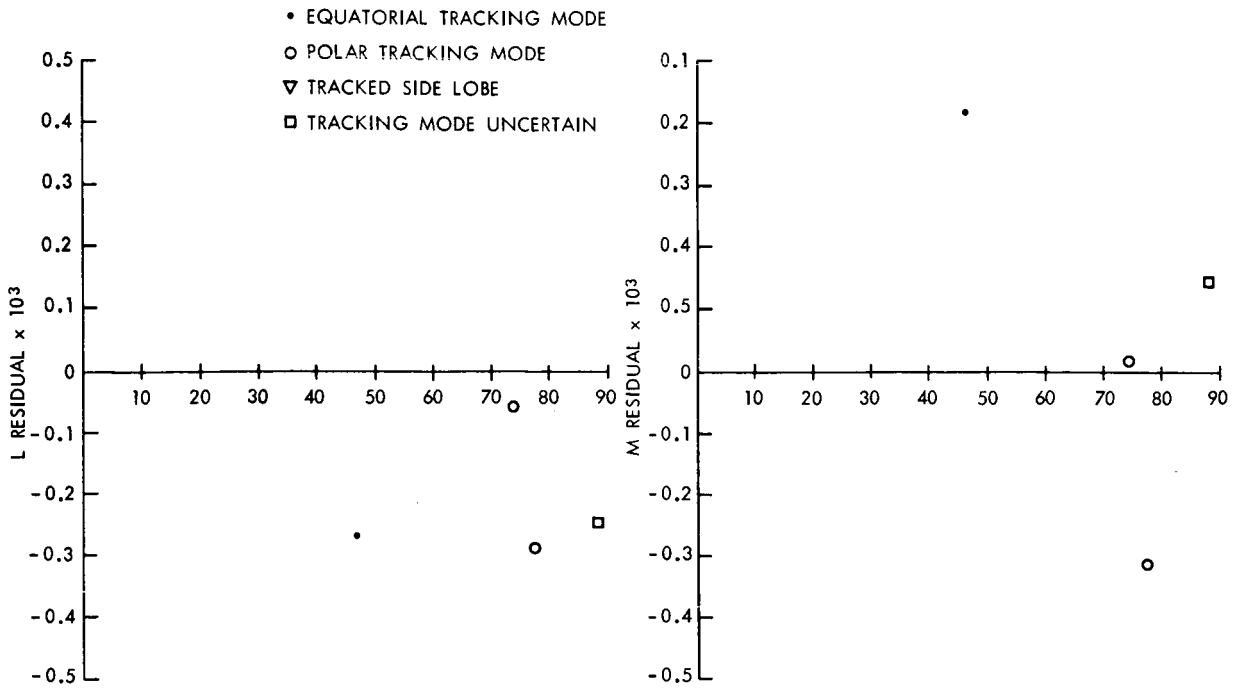

ELEVATION VS DIRECTION COSINE RESIDUAL x 10^3

k. Woomera, Australia 4 observations

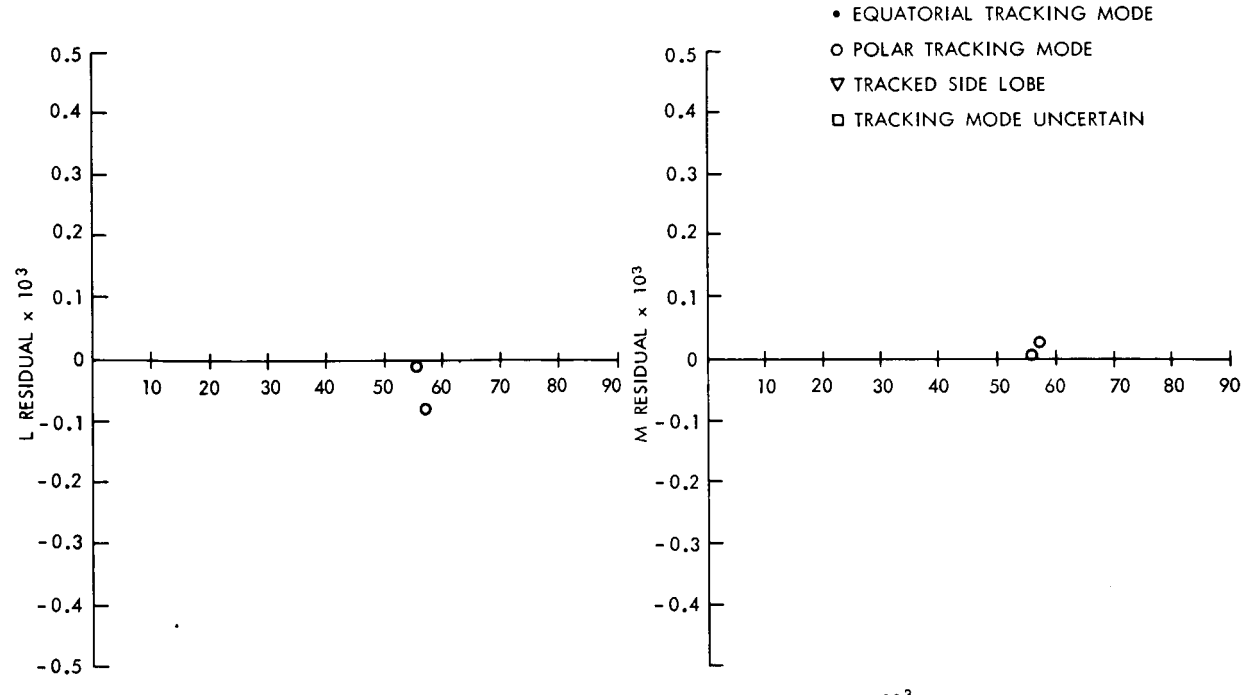

ELEVATION VS DIRECTION COSINE RESIDUAL x 10^3

l. Johannesburg, South Africa 2 observations

Figure 8.1—Plots of elevation vs. direction cosine residuals (elevation vs. $\Delta\ell \times 10^3$ and elevation vs. $\Delta m \times 10^3$) and mode of tracking (polar or equatorial).

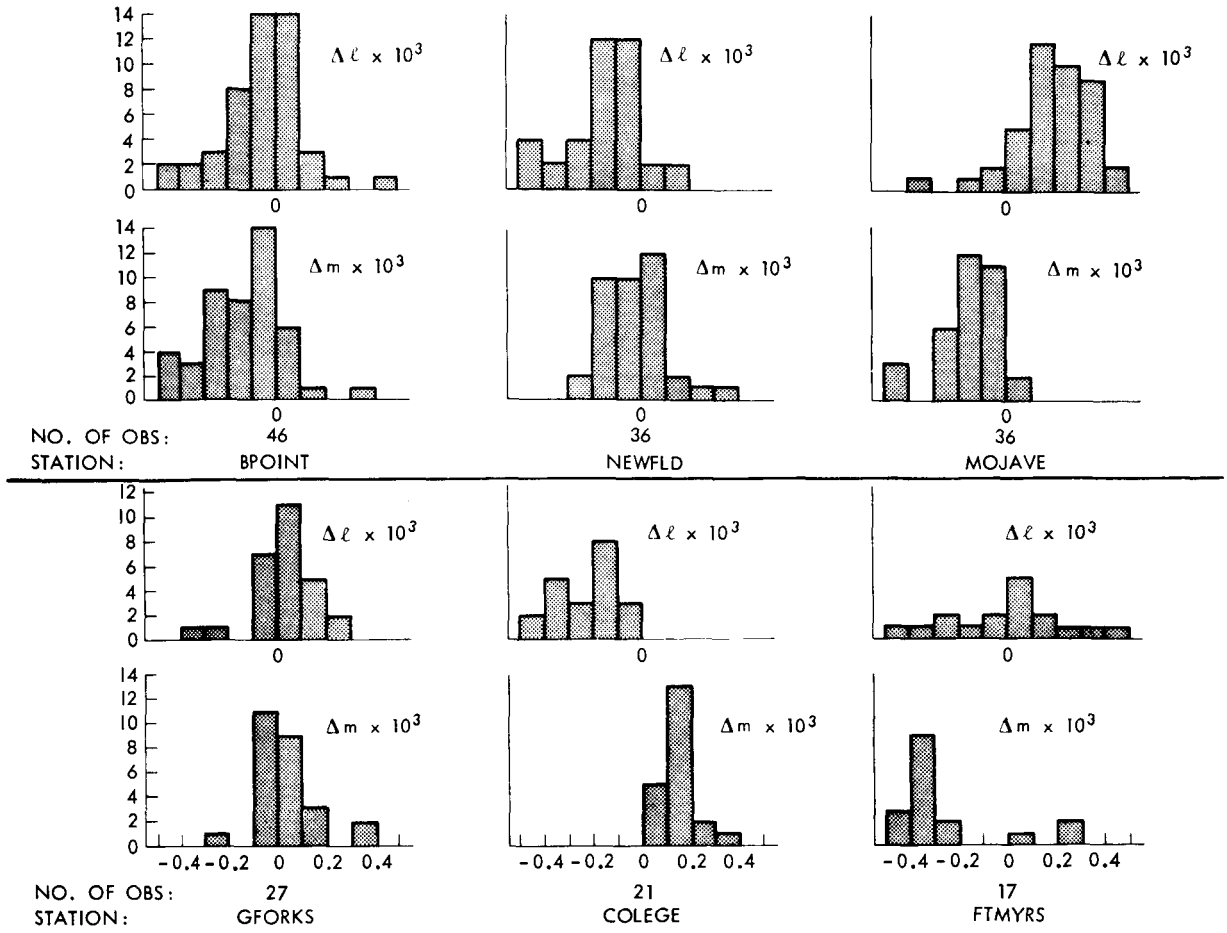

Figure 8.2a—Histogram of Minitrack residuals calculated from optically determined "standard orbit"—residuals separated by station and into $\Delta\ell$ and Δm.

and with $\Delta\ell$ and Δm separately, show no obvious biased tendency even in the separated $\Delta\ell$ and Δm histograms. A rather broad dispersion is evident in this figure, however, both for the case where $\Delta\ell$ and Δm are depicted together and when $\Delta\ell$ and Δm are depicted separately. Using a different representation (see histograms in Figure 8.2a), the residuals for some stations now show a strong biased tendency. In this case, the residuals have been separated and depicted by individual station as well as being separated into the $\Delta\ell$ and Δm histograms. In this form of presentation, the biases at Mojave and College are pronounced. However, by considering the individual dispersions by $\Delta\ell$ only and Δm only for each station, the dispersions are in general smaller than indicated by Figure 7.1 (histogram of all stations together). This suggests that if the sources of these systematic errors can be found and eliminated, there should be a corresponding reduction in the standard deviations both for the individual stations and for the data set collectively from all stations.

To illustrate the possibility of reducing the standard deviation of the data, a sample calculation was made for Mojave (Figures 8.1b and 8.2a). Considering $\Delta\ell$ and Δm both separately and together, the following mean values and standard deviations were obtained:

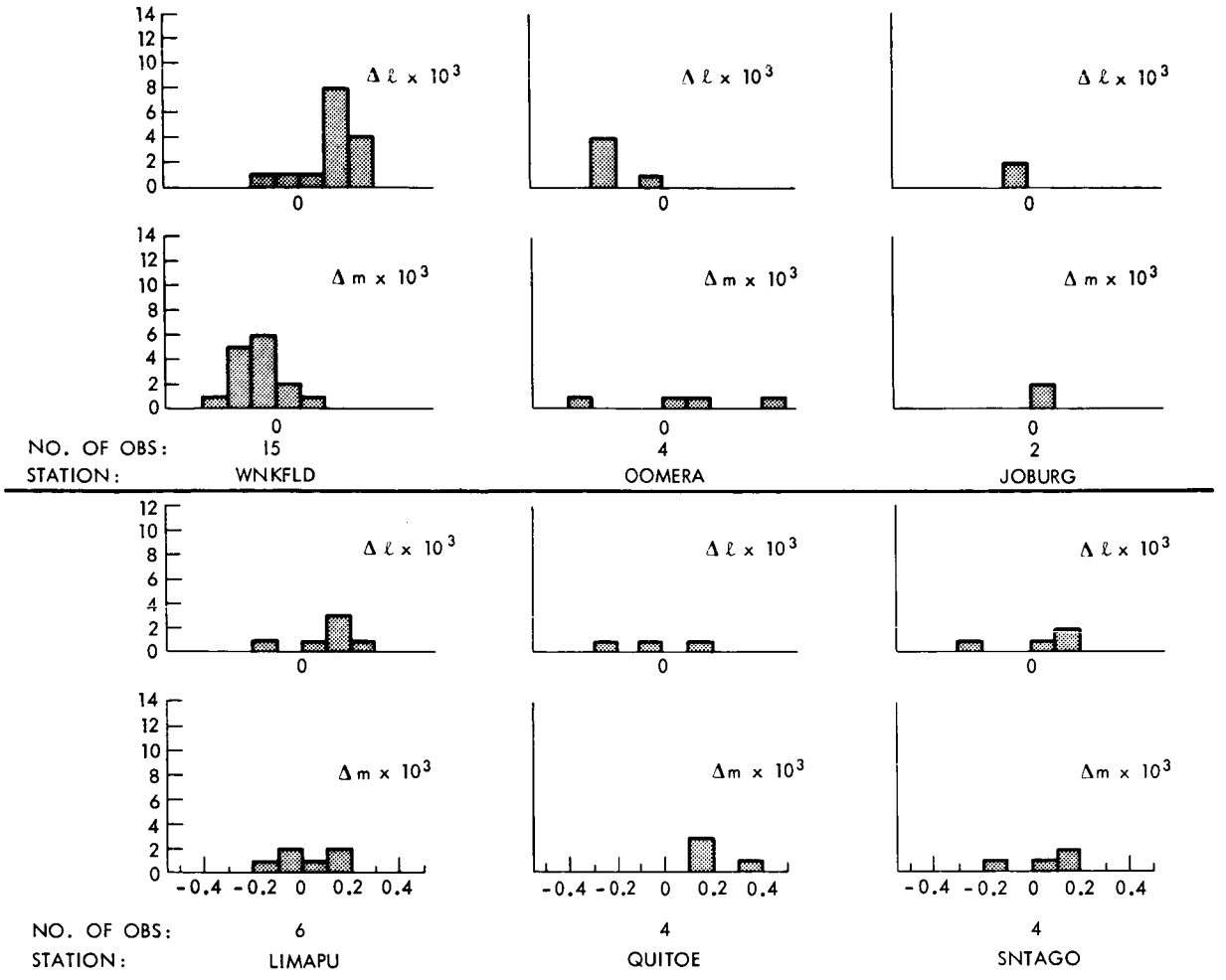

Figure 8.2b—Histogram of Minitrack residuals calculated from optically determined "standard orbit"—residuals separated by station and into $\Delta\ell$ and Δm.

	$\bar{x}$	s
$\Delta\ell$ only	$+0.18 \times 10^{-3}$	0.18×10^{-3}
Δm only	-0.16×10^{-3}	0.05×10^{-3}
$\Delta\ell + \Delta m$	$+0.01 \times 10^{-3}$	0.23×10^{-3}

It is seen that the standard deviation of $\Delta\ell$ only is approximately 25% smaller than the standard deviation of $\Delta\ell$ and Δm considered together. Next, the assumption was made that the biases for Mojave were known and that their effects caused the mean offsets of $+0.18 \times 10^{-3}$ and -0.16×10^{-3} respectively in $\Delta\ell$ and Δm. A further assumption was made that the effect of removing known biases could be approximated by subtracting the mean offsets from the corresponding residual sets. The standard deviation of the entire combined data set (ℓ and m together) was then recalculated after the offsets had been subtracted from the original residual set. The new value of the standard deviation was 0.15×10^{-3} compared to the original value of 0.23×10^{-3}, a reduction of approximately 33%. Although Mojave represented one of the most biased of the data sets used in this analysis, this

simple procedure reduced the standard deviation for Mojave to a value below the overall R.M.S. of fit of 0.19×10^{-3} for the entire data set. A further inspection of the Mojave residuals in Figure 8.1b indicates also that this bias is not primarily due to refraction dependent residuals as defined in Section 6.0 since the Δm_{polar} residuals in Figure 8.1b show a strong negative bias although they are refraction independent. Despite the indications of station biases noted in this section, however, it is felt that additional data sets should be examined before any definitive inferences of station biases can be properly made since the data set analyzed extended for only 5-1/4 days. These apparent station biases could cause an unwarranted rejection of data which may be basically good data in a computer program which employs a rejection criterion for the use of data in orbital solutions. For example, it was noted in Section 4.0 that 10% of the data from College, Alaska had residuals which exceeded 0.5×10^{-3} (the rejection criterion employed for analysis purposes in this paper).

9.0 DIFFERENCES IN ORBITS ADJUSTED USING MINITRACK DATA ONLY AND OPTICAL DATA ONLY

In order to obtain an estimate of the actual differences of position in inertial space as obtained by a Minitrack determined orbit and an optically determined orbit, trajectories obtained from the two adjusted solutions were calculated, differenced, and resolved into along track, cross track, and radial differences. The R.M.S. of fit of the orbit adjusted by Minitrack data only, not corrected for refraction or other effects, was 0.19×10^{-3} in terms of direction cosine for the 5-1/4 day arc used in the standard orbit solution. The position and velocity vectors for the epoch $01^H\ 38^M\ 22\overset{S}{.}000$ 12/31/1965 UTC which were adjusted on the basis of the 436 Minitrack observations are given in Table 9.1. The Minitrack data included observations down to 15° elevation. The R.M.S. of fit of the standard orbit adjusted by optical data only was 3".0. In both this calculation and the previous analysis, the start and end points of the Minitrack data were chosen to correspond to the equivalent start and end times of the optical data so that there would be no systematic orbital shift due to overlap effects. The along track, cross track, and radial position differences of the first and last

Table 9.1

Final Adjusted Position and Velocity Vectors at Epoch for the Minitrack Determined Orbit.

Minitrack Adjusted Position Vector	Minitrack Adjusted Velocity Vector
X: +5,690,533.8 meters Y: +1,474,657.9 meters Z: +6,013,372.3 meters	$\dot{X}$: -4,685.6272 meters/sec. $\dot{Y}$: +3,849.5020 meters/sec. $\dot{Z}$: +2,939.1288 meters/sec.
Epoch:	$01^H\ 38^M\ 22\overset{S}{.}000$ 12/31/1965 UTC
No. of Observations:	436
Arc Length:	5-1/4 days
R.M.S. of Fit:	1.906×10^{-4}

four hours of the Minitrack and optical orbits are shown in Figure 9.1 The along track difference takes the approximate form of a sine curve with a two hour period (the period of GEOS-I) with an amplitude of approximately 110 meters superimposed upon a small secular term. The secular portion of the curve has a rate of approximately 16 meters/day. Considering the optical orbit as an error free "reference orbit," the root mean square of the total position errors over the 5-1/4 day arc of the Minitrack orbit was approximately 165 meters. The Minitrack solution utilized data down to approximately 15° elevation, was not corrected for tropospheric or ionospheric refraction, and was not weighted according to elevation to compensate for any deterioration of the data at the lower elevations.

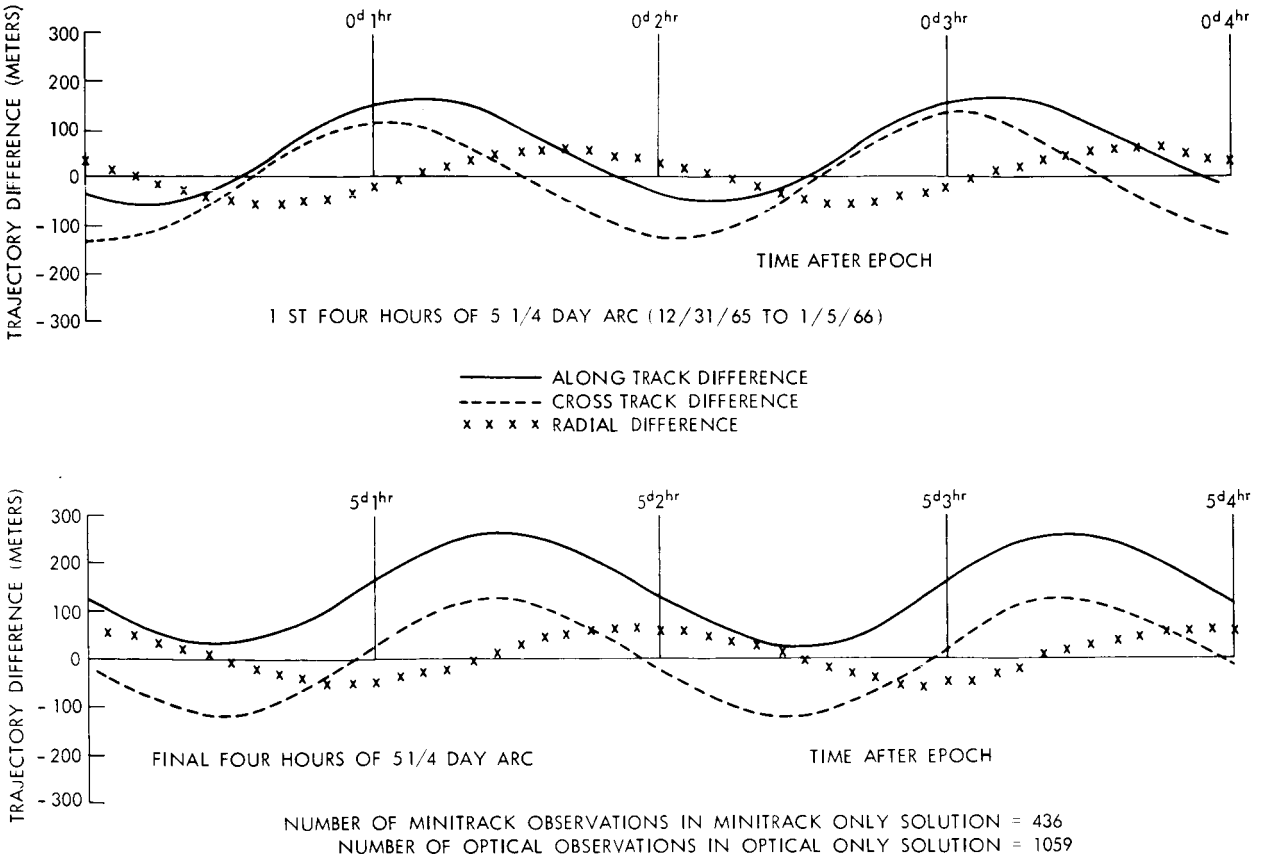

Figure 9.1—Differences between 5-1/4 day trajectories adjusted by Minitrack data only and optical data only using the SAO M-1 gravity model. (Differences are resolved along track, cross track and radially.)

10. CONCLUSIONS

It was shown that an optically determined orbit is sufficiently accurate for purposes of evaluating Minitrack data. The standard deviation of position of the Minitrack determined orbit analyzed in this report, using an optically determined orbit as a standard, was approximately 165 meters for a 5-1/4 day arc. The Minitrack determined orbit used data acquired down to 15° elevation angle. These data were not corrected for tropospheric or ionospheric refraction and were not weighted in

the solution for elevation effects. The comparatively small standard deviation of 165 meters which resulted may be attributed in a large part to a careful selection of computing tools used in the analysis. In particular, the use of an extremely accurate gravity model (SAO M1 model) and a tracking complement referred to a datum consistent with this gravity model (SAO C-5) contributed to the accuracy of the results obtained. (See Reference 16 for a more detailed analysis of gravity effects.) The relatively small standard deviation also suggests that low elevation Minitrack data when corrected for refraction effects may possibly be used with confidence in orbital solutions. The technique which was developed in this paper to separate out refraction dependent residuals from refraction independent residuals presents one possible approach to the development of a method of self-calibrating out residual refraction effects which remain after nominal refraction corrections have been applied to the data.

The use of optical data as an independent data set revealed systematic offsets of the residuals at certain Minitrack sites. The use of such an independent data set could be effectively used to determine the calibration coefficients for the individual Minitrack stations and to investigate the feasibility of using the Minitrack data itself for self-calibration purposes.

REFERENCES

1. NASA-GSFC Operations Plan 11-65 Geodetic Satellite (GEOS-A), August 1965, X-535-345.
2. Simas, V. R.—Unpublished Notes
3. Kaula, W. M., "Celestial Geodesy," March 1962, NASA TN D-1155.
4. SAO Special Report No. 200, Vol. 1, "Geodetic Parameters for a 1966 Smithsonian Institution Standard Earth," 1966.
5. Köhnlein, W., "The Earth's Gravitational Field as Derived from a Combination of Satellite Data with Gravity Anomalies," prepared for the XIV General Assembly, International Union of Geodesy & Geophysics, International Association of Geodesy, September 25—October 7, 1967, Lucerne, Switzerland.
6. New Mexico State University, Physical Science Laboratory, "Inspection of the 136.5 MC Minitrack STADAN Antennas at Santiago, Chile, S. A.," January 1965.
7. NASA, "Handbook of Operating Instructions for Minitrack and Telemetry Systems," January 12, 1961.
8. Bendix Corp., "Instruction Manual for 136 MC Minitrack Interferometer System," Vol. I of II.
9. Bendix Radio, "Instruction Book for Minitrack Satellite Tracking Unit Designed by U. S. Naval Research Laboratory (108 MC)."
10. NASA, Project Vanguard, Tracking and Guidance Branch (compilation), "Minitrack System Training Manual (Revised September 1958)."

11. Astro-Geo-Astro, "Minitrack Calibration System Model 2, Ground Equipment Instruction Manual."

12. R. H. Gooding, "Orbit Determination from Minitrack Observations."

13a. "GEOS Integrated Investigation Plan," September 23, 1965, prepared for NASA by System Sciences Corporation.

13b. "GEOS-A Mission Plan," September 16, 1965, prepared for NASA by System Sciences Corporation.

14. "Technical Plan for a National Geodetic Satellite Program," March 1965, submitted to NASA by the John Hopkins University Applied Physics Laboratory.

15. Berbert, J. H., Oosterhout, J. D., Engels, P. D., and Habib, E. J., "Minitrack Calibration System," March-April, 1963, Photographic Science and Engineering, Vol. 7, No. 2.

16. Lerch, F. J., Marsh, J. G., O'Neill, B., "Gravity Model Comparison Using GEOS-I Long Arc Orbital Solutions," December 1967, Goddard Space Flight Center Document X-552-67-71.

17. Watkins, E. R., Jr., Private Communication, Goddard Space Flight Center, Computation Division, Operational Computing Branch.

18. Vonbun, F. O., "Corrections for Atmospheric Refraction at the NASA Minitrack Stations," August 1962, NASA TN-D-1448.

19. "Minitrack Tracking Data Reduction and Control."

20. Sapper, Larry W., GSFC, Data Operations Branch Memoranda for Record:

    a. "Reduction of Raw Minitrack Phase Angle Data to Direction Cosines ℓ and m" 11/24/65 revised 10/11/65.

    b. "Addendum to Memorandum for Period:
    Reduction of Raw Minitrack Phase Angle Data to Direction Cosines ℓ and m" 2/16/66.

    c. "Interpolation of the Medium and Course Phase Angles in the Reduction of Minitrack Data" 3/1/66.

21. Evans, C. H. and Cole, I. J., GSFC, Advanced Orbital Programming Branch AOPB Systems Manual Program Description

    a. "F036 Ionosphere Data Load" 11/65

    b. "F037 Ionosphere Data Search" 11/65

22. Cole, I. J., GSFC, Advanced Orbital Programming Branch AOPB Systems Manual Program Description "F116 ℓ, m, ρ, $\dot{\rho}$ corrector for Ionosphere Refraction," 11/65.

23. Cannaday, D. J., Private Communication, Goddard Space Flight Center, Computation Division, Operational Computing Branch.

Appendix A

BRIEF DESCRIPTION OF THE 136 MC MINITRACK INTERFEROMETER TRACKING SYSTEM

The basic Minitrack configuration consists of an antenna field of 13 antennas arranged as shown in Figure A1. In addition to the antenna system, there is an operations building housing the electronic systems. A MOTS 40 inch focal length camera is located at the exact center of the fine beam arrays of the antenna system. This camera is normally used for calibrating the antenna system by photographing an airborne flashing light beacon against a background of stars while the antenna system is simultaneously receiving a 136 MC radio signal from the same airborne source. Since theoretically the physical location of the MOTS camera and the antenna system center are

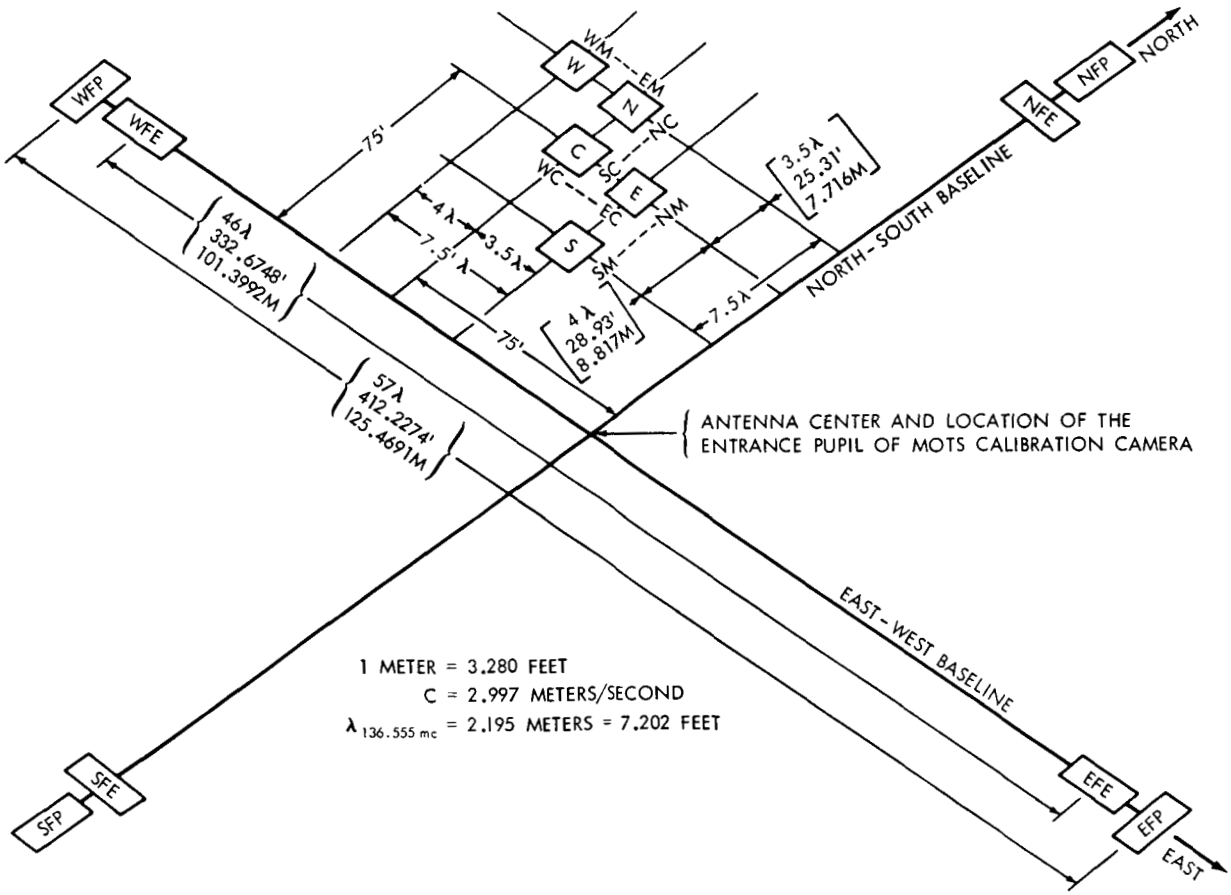

Figure A1—136 MC. Minitrack antenna layout.

identical, a unique system is available for intercomparing the two distinct tracking systems types.

The electronics of the Minitrack interferometer system are designed to locate satellites transmitting on 1000 separate frequencies ranging from 136.000 MC to 136.999 MC in 1 KC steps. The tracking is performed in a completely passive mode. The possibility of extending this range to 138 MC is currently being considered.

The antenna system is designed to be highly directive resulting in a high signal gain. There are two possible modes of tracking, the "equatorial" mode and the "polar" mode. The wave length dimensions displayed in Figure A1 are based upon a received signal whose frequency is 136.555 MC.

The antenna arrays located at the ends of the North-South and East-West baselines are used in sets of four for each of the two tracking modes and are abbreviated as follows:

Group 1 – Equatorial Tracking Mode

Equatorial Fine Beam Arrays

NFE	North Fine Equatorial
SFE	South Fine Equatorial
EFE	East Fine Equatorial
WFE	West Fine Equatorial

Group 2 – Polar Tracking Mode

Polar Fine Beam Arrays

NFP	North Fine Polar
SFP	South Fine Polar
EFP	East Fine Polar
WFP	West Fine Polar

The distance between NFE and SFE is the same as indicated between WFE and EFE. Also, the distance between NFP and SFP is the same as indicated between EFP and WFP.

The reception pattern of Group 1 (Equatorial Fine Beam) is shown on the left side of Figure A2. The reception pattern of Group 2 (Polar Fine Beam) is shown on the right side of the same figure. These two groups comprise the accurate portion of the antenna system. The individual stations can electronically switch between the Polar and Equatorial modes of tracking very quickly so that both modes of tracking are possible on the same pass of a spacecraft. The actual shape of the wedge or fan-shaped pattern of the fine beam is defined by the locus of points where the signal from the satellite's Minitrack beacon drops 3 decibels from the zenith signal. Under normal conditions, the satellite is only tracked when it is located with this wedge-shaped fine beam. Tracking is usually further restricted to a maximum zenith distance of 20° in the long beam direction of this pattern in order to minimize refraction effects. A typical reception pattern for the EFE array in the East-West direction at the Minitrack station at Santiago, Chile is shown in Figure A3.

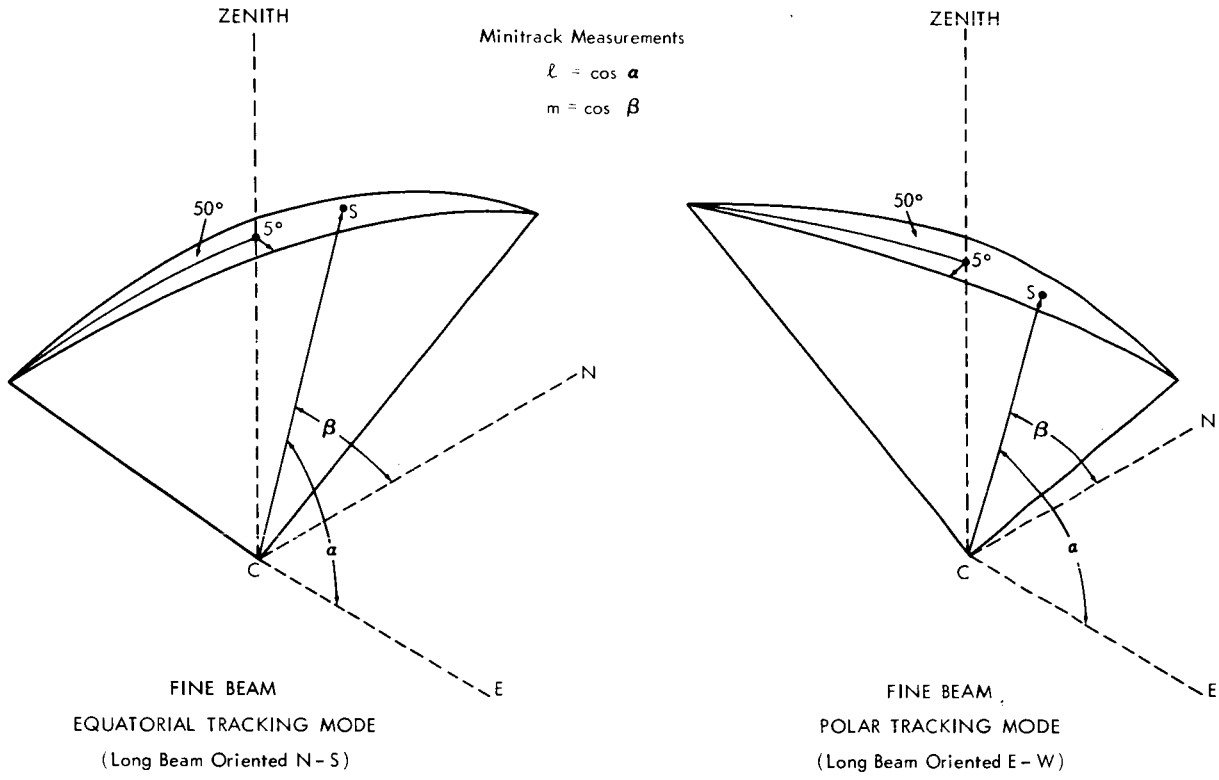

Figure A2—Approximate reception pattern of the fine beam of the 136 MC Minitrack antenna array.

In order to calculate the direction cosines of a spacecraft, it is necessary to know the absolute phase difference of the signal as received simultaneously by a pair of the fine beam antennas, for example, WFE and EFE. Since only relative phase differences of the signal can be measured as received by the fine beam pairs, it is necessary to introduce five additional arrays to resolve these phase difference ambiguities which arise. The ambiguity antennas are labeled in Figure A1 as W, N, C, E, S (West, North, Common, East, and South respectively). This group of five antennas can be used to resolve the ambiguities for both the Group 1 and Group 2 fine beam arrays. The W-N and E-S combinations are used for East-West medium and North-South medium resolution respectively. The N-C and C-E combinations are used for North-South and East-West course resolution respectively. In each case, the combinations are separated by 4 and 3.5 wave lengths so that the differences in separation of the medium and course combinations used to resolve either

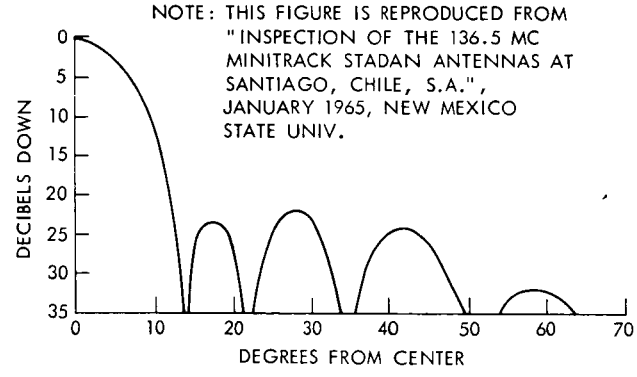

Figure A3—Antenna pattern for east fine equatorial Minitrack antenna at Santiago, Chile.

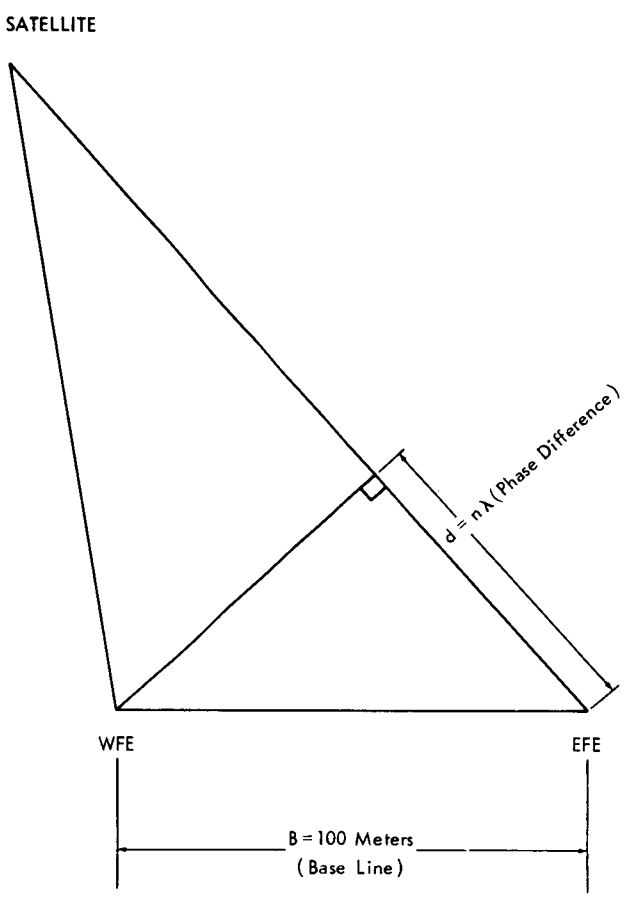

Figure A4—Simplified geometry of satellite 136 MC Minitrack beacon signal as received by the west fine equatorial and east fine equatorial antenna arrays.

North-South or East-West ambiguities, are only 1/2 of a wave length.

The electronics of the Minitrack system divide the 360 electrical degrees phase measurement into 1000 parts or 0.36 electrical degrees. This measurement represents the upper precision limit of the equipment. If it is assumed that the fine beam baseline is approximately 100 meters (see Figure A4) then the resulting accuracy in terms of space angle may be estimated approximately by the following considerations. The direction cosine ℓ (considering the East-West baseline) is related to the electrical phase angle by the equation.

$$\ell = \cos\alpha = \frac{d}{B} = \frac{n\lambda}{B}$$

$$= \frac{\phi}{2\pi}\frac{\lambda}{B}$$

ϕ = electrical angle in radians

λ = signal wave length

$\cong$ 2.2 meters at 136.555 MC

B = antenna separation distance or baseline length

$\cong$ 100 meters

d = phase difference in linear measure

n = phase difference in number of wave lengths of signal

If ϕ is measured in degrees, this becomes

$$\ell = \cos\alpha = \frac{\phi}{360^\circ}\frac{2.2}{100}$$

To find the error in ℓ and α,

$$\Delta\ell = -\sin\alpha\,\Delta\alpha = \frac{2.2}{360 \times 100}\Delta\phi$$

$$= \frac{2.2}{3.6} \times 10^{-4}\,\Delta\phi$$

If $\Delta\ell$ = 0.36 degrees, then

$$\Delta\ell \simeq -\sin\alpha\,\Delta\alpha = \frac{2.2}{3.6} \times 0.36 \times 10^{-4}$$

$$2.2 \times 10^{-5}$$

For a near overhead pass, $\sin\alpha \simeq 1$. Neglecting the minus sign

$$\Delta\alpha = 2.2 \times 10^{-5} \text{ radians}$$

$$= 2.2 \times 10^{-5} \times \left(2 \times 10^{5}\right)''$$

$$= 4''.4$$

Appendix B

PREPROCESSING OF OPTICAL OBSERVATIONS

1. Preprocessing of Optical Data

The first step in the processing of optical observations is usually performed by the observing source. This consists of developing a plate or film, identifying the image or images of the satellite and the images of several reference stars whose right ascensions and declinations are well known. The initial measurements of both satellite images and reference stars consist of linear rectangular coordinates. From the knowledge of the spherical coordinates of the reference stars, the right ascesions and declinations of the satellite images may be calculated. These coordinates as received by the preprocessor may be referred to the mean equator and equinox of date, true equator and equinox of date, or mean equator and equinox of some standard epoch.

The preprocessor then transforms these observations to a common coordinate system. Currently, the preprocessor transforms all right ascensions and declinations to the true equator and equinox of the epoch of the observations being processed. If the observations were originally referred to the mean equator and equinox of a particular epoch, it is only necessary to precess from that epoch to the epoch of the observations. However, if they were referred to the true equator and equinox of a particular epoch, it is necessary first to transform them to the mean equator and equinox of that same epoch and then precess to the epoch of the observations.

Finally, a transformation must be made from the mean equator and equinox of the epoch of the observations of the true equator and equinox of the epoch of the observations.

2. Nutation

The transformation from the true equator and equinox of date to the mean equator and equinox of date is

$$Y = NX$$

where

$$Y = \begin{bmatrix} \cos\delta_m & \cos\alpha_m \\ \cos\delta_m & \sin\alpha_m \\ \sin\delta_m & \end{bmatrix}$$

$$X = \begin{bmatrix} \cos\delta_T \cos\alpha_T \\ \cos\delta_T \sin\sigma_T \\ \sin\delta_T \end{bmatrix}$$

$$N = \begin{bmatrix} 1 & +\Delta\psi \cos\epsilon_m & +\Delta\psi \sin\epsilon_m \\ -\Delta\psi \cos\epsilon_m & 1 & +\Delta\epsilon \\ -\Delta\psi \sin\epsilon_m & -\Delta\epsilon & 1 \end{bmatrix}$$

and

α_m, δ_m = right ascension and declination referred to mean equator and equinox of date

α_T, δ_T = right ascension and declination referred to true equator and equinox of date

ϵ_m = mean obliquity of date

$\Delta\psi$ = nutation in longitude

$\Delta\epsilon$ = nutation in obliquity

The inverse transformation is simply:

$$X = N^{-1} Y = N^T Y$$

3. Precession

The transformation from the mean equator and equinox of 1950.0 to the mean equator and equinox of an arbitrary epoch t1 is

$$Y = PX$$

where

$$Y = \begin{bmatrix} \cos\delta_{t1} \cos\alpha_{t1} \\ \cos\delta_{t1} \sin\alpha_{t1} \\ \sin\delta_{t1} \end{bmatrix}$$

$$X = \begin{bmatrix} \cos\delta_{1950.0} \cos\alpha_{1950.0} \\ \cos\delta_{1950.0} \sin\alpha_{1950.0} \\ \sin\delta_{1950.0} \end{bmatrix}$$

$$P = \begin{bmatrix} (\cos z \cos \theta \cos \zeta - \sin z \sin \zeta) & (-\cos z \cos \theta \sin \zeta - \sin z \cos \zeta) & (-\cos z \sin \theta) \\ (\sin z \cos \theta \cos \zeta + \cos z \sin \zeta) & (-\sin z \cos \theta \sin \zeta + \cos z \cos \zeta) & (-\sin z \sin \theta) \\ (\sin \theta \cos \zeta) & (-\sin \theta \sin \zeta) & (\cos \theta) \end{bmatrix}$$

The inverse transformation is

$$X = P^{-1} Y = P^{T} Y$$

Since the expression for z, θ, ζ are tied to 1950.0 as an epoch, the precession between two different epochs, neither of which is 1950.0, must be performed in two steps, using 1950.0 as an intermediary epoch. The above expression for P is rigorous. There are simple 3rd degree polynomials in time derived by Newcomb which permit the calculation of z, θ, and ζ. There exists an even simpler form of the matrix P which permits the calculation of its elements by means of 3rd degree polynomials expressed directly in terms of the variable t (time). This simplification bypasses the necessity of calculating the sines and cosines of the angles z, θ, and ζ. These simplified matrix elements are derived by expanding the sines and cosines of z, θ, and ζ, contained in the elements of P into a series, performing the necessary multiplications and dropping terms exceeding the 3rd degree. The appropriate polynomial expressions in t are then substituted into the remaining expressions containing z, θ, and ζ. After the necessary multiplications are again performed, all terms in t higher than the 3rd degree are dropped. The final expression for P then consists simply of 9 elements in terms of a 3rd degree polynomial in time.

Appendix C

FORCE MODELS USED IN NONAME

1. Force Models

The data reduction program in its present form incorporates four force models. These are:

1. The earth's gravitational field
2. The solar and lunar gravitational perturbations
3. Solar radiation pressure
4. Atmospheric drag

The program is designed such that the gravitational coefficients and pertinent physical characteristics of satellites, such as reflectivity, cross-sectional area mass, and drag coefficient can be simply changed through card input or block data statement.

2. The Earth's Gravitational Field

The formulation of the geopotential used is:

$$u = \frac{GM}{r}\left\{1 + \sum_{n=2}^{k}\sum_{m=0}^{n}\left(\frac{a}{r}\right)^n P_n^m(\sin\phi)\left[C_{nm}\cos m\lambda + S_{nm}\sin m\lambda\right]\right\} \qquad \text{(C1)}$$

where

G is the universal gravitational constant

M is the mass of the earth

r is the geocentric satellite distance

a is the earth's mean equatorial radius

ϕ is the sub-satellite latitude

λ is the sub-satellite east longitude

$P_n^m(\sin\phi)$ is the associated spherical harmonic of degree n and order m.

The design of the potential function requires that normalized gravitational coefficients $C_{n,m}$ and $S_{n,m}$ be used. The program is presently capable of accepting coefficients up to (20, 20) or any subset of these.

The SAO M-1 earth gravitational model (Reference 1) modified by the GEOS-I resonant harmonics ($\bar{C}_{13,12}$, $\bar{S}_{13,12}$, $\bar{C}_{14,12}$, $\bar{S}_{14,12}$, $\bar{C}_{15,12}$, $\bar{S}_{15,12}$) (Reference 2) is listed in Table C1. These coefficients have been used extensively in the NONAME orbit determination program for the reduction of GEOS-I optical and electronic data. The same data sets have been reduced using various other gravity models. An intercomparison of the results can be found in Reference 3.

The transformation of the geopotential in earth-fixed coordinates (r, ϕ, λ) to gravitational accelerations in inertial coordinates (x, y, z) is accomplished as follows:

$$\ddot{x}_{\oplus} = \frac{\partial u}{\partial r}\frac{\partial r}{\partial x} + \frac{\partial u}{\partial \phi}\frac{\partial \phi}{\partial x} + \frac{\partial u}{\partial \lambda}\frac{\partial \lambda}{\partial x}\,; \qquad \ddot{y}_{\oplus}\,, \qquad \ddot{z}_{\oplus} \tag{C2}$$

where the subscript "$\oplus$" denotes accelerations due to the earth's field.

3. Solar and Lunar Gravitational Perturbations

The perturbations caused by a third body, e.g., the sun or moon, on a satellite orbit are treated by defining a disturbing function R* which can be treated as the potential function U. For the solar perturbation $R_{\odot}$ takes the form

$$R_{\odot} = \frac{GMm_{\odot}}{r_{\odot}}\left[\left(1 - \frac{2r}{r_{\odot}}S + \frac{r^2}{r_{\odot}^2}\right)^{-1/2} - \frac{rS}{r_{\odot}}\right] \tag{C3}$$

where

$$S = \cos\left(\vec{r}, \vec{r}_{\odot}\right)$$

$m_{\odot}$ is the mass of the sun in earth masses

$\vec{r}_{\odot}$ is the geocentric position vector of the sun

$r_{\odot}$ is the geocentric distance to the sun

$\vec{r}$ is the geocentric position vector of the satellite

r is the geocentric distance to the satellite

G is the universal gravitational constant

M is the mass of the earth

*Kozai, Y, Smithsonian Astrophysical Observatory Special Report 22, pp. 7-10.

Table C1

SAO M-1 Harmonic Coefficients (Normalized).

n	m	$\bar{C} \times 10^6$	$\bar{S} \times 10^6$	n	m	$\bar{C} \times 10^6$	$\bar{S} \times 10^6$
2	0	-484.1735		8	2	0.026	0.039
2	1			8	3	-0.037	0.004
2	2	2.379	-1.351	8	4	-0.212	-0.012
				8	5	-0.053	0.118
3	0	0.9623		8	6	-0.017	0.318
3	1	1.936	0.266	8	7	-0.0087	0.031
3	2	0.734	-0.538	8	8	-0.248	0.102
3	3	0.561	1.620				
				9	0	0.0122	
4	0	0.5497		9	1	0.117	0.012
4	1	-0.572	-0.469	9	2	-0.0040	0.035
4	2	0.330	0.661				
4	3	0.851	-0.190	10	00	0.0118	
4	4	-0.053	0.230	10	01	0.105	-0.126
				10	02	-0.105	-0.042
5	0	0.0633		10	03	-0.065	0.030
5	1	-0.079	-0.103	10	04	-0.074	-0.111
5	2	0.631	-0.232				
5	3	-0.520	0.007	11	00	-0.0630	
5	4	-0.265	0.064	11	01	-0.053	0.015
5	5	0.156	-0.592				
				12	00	0.0714	
6	0	-0.1792		12	01	-0.163	-0.071
6	1	-0.047	-0.027	12	02	-0.103	-0.0051
6	2	0.069	-0.366	12	12	-0.031	0.0008
6	3	-0.054	0.031				
6	4	-0.044	-0.518	13	00	0.0219	
6	5	-0.313	-0.458	13	12	-0.06769	0.06245
6	6	-0.040	-0.155	13	13	-0.059	0.077
7	0	0.0860					
7	1	0.197	0.156	14	00	-0.0332	
7	2	0.364	0.163	14	01	-0.015	0.0053
7	3	0.250	0.018	14	11	0.0002	-0.0001
7	4	-0.152	-0.102	14	12	0.00261	-0.02457
7	5	0.076	0.054	14	14	-0.014	-0.003
7	6	-0.209	0.063				
7	7	0.055	0.096	15	09	-0.0009	-0.0018
				15	12	-0.07473	-0.01026
8	0	0.0655		15	13	-0.058	-0.046
8	1	-0.075	0.065	15	14	0.0043	-0.0211

The normalized coefficients ($\bar{C}_{n,m}$, $\bar{S}_{n,m}$) are related to the denormalized coefficients ($C_{n,m}$, $S_{n,m}$) as indicated below:

$$C(n, m) = \left[(n-m)!\,(2n+1)k/(n+m)!\right]^{1/2} \bar{C}(n, m)$$

$$S(n, m) = \left[(n-m)!\,(2n+1)k/(n+m)!\right]^{1/2} \bar{S}(n, m)$$

$k = 1$ when $m = 0$

$k = 2$ when $m \neq 0$

The acceleration of the satellite due to the sun is then

$$\ddot{x}_{\odot} = \frac{\partial R_{\odot}}{\partial r}\frac{\partial r}{\partial x} + \frac{\partial R_{\odot}}{\partial \phi}\frac{\partial \phi}{\partial x} + \frac{\partial R_{\odot}}{\partial \lambda}\frac{\partial \lambda}{\partial x} \; ; \qquad \ddot{y}_{\odot} \; ; \qquad \ddot{z}_{\odot} \tag{C4}$$

where λ and ϕ are the longitude and latitude of the satellite respectively. The lunar perturbation is found from Equation C3 by substituting the lunar mass and distance for those of the sun.

The lunar and solar ephemerides are computed internal to the program. These positions are computed at ten equal intervals over each five day period and least squares fit to a fourth order polynomial in time about the midpoint of the five day period. The positions of these bodies are then determined at each data point by evaluating the polynomial at the observation time.

4. Solar Radiation Pressure

The acceleration acting on a satellite due to solar radiation pressure is formulated as follows.*

$$\ddot{x}_{RAD} = -\frac{AP_{\odot}}{m}\gamma\nu L_x \; ; \qquad \ddot{y}_{RAD} \, , \qquad \ddot{z}_{RAD} \tag{C5}$$

where

L is the inertial unit vector from the geocenter to the sun and whose components are L_x, L_y, L_z.

A is the cross sectional area of the satellite

m is the satellite mass

γ is a factor depending on the reflective characteristics of the satellite

ν is the eclipse factor such that:

$$\nu = \begin{cases} 0 \text{ when satellite is in earth's shadow} \\ 1 \text{ when satellite is illuminated by the sun} \end{cases}$$

$P_{\odot}$ is the solar radiation pressure in the vicinity of the earth,

$$4.5 \times 10^{-6} \frac{\text{Newton}}{m^2}$$

At present, it is assumed that the satellite is specularly reflecting with reflectivity, ρ, and thus

$$\gamma = (1 + \rho) \, . \tag{C6}$$

*H. Koelle, Handbook of Astronomical Engineering pp. 8-33, McGraw-Hill, 1961.

The vector $\hat{L}$ and the eclipse factor are determined from the solar ephemeris subroutine previously described, the satellite ephemeris, and involve the approximation of a cylindrical earth shadow.

5. Atmospheric Drag

The atmospheric decelerations are computed as follows:

$$\ddot{x}_{DRAG} = -\frac{\rho C_D A v v_x}{2m} ; \qquad \ddot{y}_{DRAG}, \qquad \ddot{z}_{DRAG} \tag{C7}$$

where

ρ is the ambient atmospheric density

C_D is the satellite drag coefficient

A is the projected area of the satellite on a plane perpendicular to direction of motion

m is the satellite mass.

The velocity vector $\vec{v}$ given in inertial coordinates by

$$\vec{v} = v_x \hat{i} + v_y \hat{j} + v_z \hat{k} \tag{C8}$$

can be chosen to be either the velocity relative to the atmosphere which implies that the atmosphere rotates with the earth or the inertial velocity which assumes that the atmosphere is static. Presently, the former assumption is made.

The density, ρ, is computed from the 1962 U. S. Standard Atmosphere.

References—Appendix C

1. Lundquist, C. A., Veis, G., "Geodetic Parameters for a 1966 Smithsonian Institution Standard Earth," SAO Special Report No. 200, Vol. 1.
2. Köhnlein, W., The Earth's Gravitational Field as Derived from a Combination of Satellite Data with Gravity Anomalies, Prepared for XIV General Assembly, International Union of Geodesy and Geophysics, International Association of Geodesy, October 1967.
3. Lerch, F. J., Marsh, J. G., O'Neill, B., "Gravity Model Comparison Using GEOS-I Long Arc Orbital Solutions," GSFC Document X-552-67-71, December 1967.

Appendix D

TRACKING STATION COORDINATES

1. Datum Parameters and Station Coordinates

For the purpose of long-arc satellite data reduction and intercomparison all GEOS-I participating tracking stations have been transformed to a common datum. The common datum selected is the SAO Standard Earth C-5 model (Semi-major axis = 6378165 meters, flattening coeff. = 298.25) (Reference 1) in which the Baker-Nunn station positions are used as the controlling stations for all other stations to be transformed. Descriptions and formulations to effect the transformations from major and isolated datums are presented in Reference 2. The transformation of local datum station coordinates to a common center of mass reference system is important to be performed since the datum shifts are quite large. For example, on the North American Datum the center of mass shift to the C-5 Standard Earth is approximately 250 meters. The center of mass coordinates of the SAO C-5 Baker-Nunn stations are assessed by SAO to have approximately 20 meter accuracy.

In order to effect any transformation, the parameters of the original datums must be known as well as the geodetic latitude, longitude and height. Table D1 provides a listing of the original datums and their parameters on which the stations were originally surveyed. Tables D2 to D11 list alternately the original surveyed ellipsoidal positions and the SAO C-5 ellipsoidal positions for over 100 GEOS-I tracking stations that have been used in the long arc intercomparison effort. These tables contain symbols designating the source of original station coordinates. The symbols are defined in Section 2 with a list of source information. The C-5 positions for 1TANAN and MADGAR (Reference 3) have been derived by the station estimation technique contained in the Orbit Determination Program NONAME. Tables D12 to D21 provide a listing of the proper station names from which the six letter designations have been derived.

2. Sources

The following sources were used to obtain the original datum positions:

Symbol	Source
A	Geodetic Parameters for a Standard Earth Obtained from Baker-Nunn Observations; September 1966; Smithsonian Astrophysical Observatory.
B	Goddard Directory of Tracking Station Locations; August 1966; Goddard Space Flight Center.
C	NWL-8 Geodetic Parameters Based on Doppler Satellite Observations; July 1967; R. Anderle and S. Smith, Naval Weapons Laboratory.

Since the above official documents did not contain all those positions that were to be transformed, it was necessary to contact other sources for the positions of the remaining stations. These sources are:

Symbol	Source
D	Private communication with personnel at SAO; K. Haramondanis; B. Miller; A. Girnius.
E	Private communication with 1381 Geodetic Survey Squadron, USAF; S. Tischler.
F	Private communication with personnel at USC&GS; B. Stevens.
G	Private communication with personnel at U. S. Army Engineers Topographic Laboratories; L. Gambino.
H	Private communication with NASA Space Science Data Center; J. Johns; D. Tidwell.
I	General Station Data Sheet—GEOS-A Project Manager NASA Headquarters.

Table D1

Parameters of Original Datums.

Datum Name	Semi-Major Axis (meters)	1/f
North American (N.A.)	6378206.4	294.9787
European	6378388.0	297.0
Tokyo	6377397.2	299.1528
Argentinean	6378388.0	297.0
Mercury	6378166.0	298.3
Madagascar	6378388.0	297.0
Australian Nat'l.	6378160.0	298.25
Old Hawaiian	6378206.4	294.9787
Indian	6377276.3	300.8017
Arc (Cape)	6378249.1	293.4663
1966 Canton Astro	6378388.0	297.0
Johnston Island 1961	6378388.0	297.0
Midway Astro 1961	6378388.0	297.0
Navy Iben Astro 1947	6378206.4	294.9787
Provisional DOS Astro 1962, 65 Allen Sodano Lt.	6378388.0	297.0
1966 SECOR ASTRO	6378388.0	297.0
Viti Levu 1916	6378249.1	293.4663
CORREGO ALEGRE	6378206.4	294.9787
USGS 1962 ASTRO	6378206.4	294.9787
BERNE	6377397.2	299.1528

Table D2

SAO Optical Source A.

Source	Name	Station No.	Latitude	Longitude	Geodetic Height (meters)	Datum
	1ORGAN	9001	32°25'24!56	253°26'51!17	1649	N.A.
			32 25 24.70	253 26 48.29	1610	C-5
	1OLFAN	9002	-25 57 33.85	28 14 53.91	1562	Arc (Cape)
			-25 57 37.67	28 14 51.45	1560	C-5
	WOOMER	9003	-31 06 07.26	136 46 58.70	185	Australian
			-31 06 04.14	136 47 01.93	158	C-5
	1SPAIN	9004	36 27 51.24	353 47 41.47	7	European
			36 27 46.68	353 47 36.55	56	C-5
	1TOKYO	9005	35 40 11.08	139 32 28.22	58	Tokyo
			35 40 23.03	139 32 16.42	84	C-5
	1NATOL	9006	29 21 38.90	79 27 25.61	1847	European
			29 21 34.38	79 27 27.05	1855	C-5
	1QUIPA	9007	-16 28 05.09	288 30 22.84	2600	N.A.
			-16 27 58.04	288 30 24.02	2479	C-5
	1SHRAZ	9008	29 38 17.96	52 31 11.80	1578	European
			29 38 13.59	52 31 11.20	1561	C-5
	1CURAC	9009	12 05 21.55	291 09 42.55	23	N.A.
			12 05 24.93	291 09 43.97	-33	C-5
	1JUPTR	9010	27 01 13.00	279 53 12.92	26	N.A.
			27 01 14.23	279 53 12.95	-36	C-5
	1VILDO	9011	-31 56 36.53	294 53 39.82	598	Argentinean
			-31 56 36.35	294 53 36.11	636	C-5
	1MAUIO	9012	20 42 37.49	203 44 24.11	3027	Old Hawaiian
			20 42 25.66	203 44 33.23	3027	C-5
	AUSBAK	9023	-31 23 30.82	136 52 39.02	164	Australian
			-31 23 27.69	136 52 42.23	137	C-5
	OSLONR	9426	60 12 40.38	10 45 08.74	585	European
			60 12 38.88	10 45 02.26	573	C-5
I	NATALB*	9029	-05 55 50.00	324 50 18.00	112	N.A.
			-05 55 43.49	324 50 21.30	45	C-5
D	AGASSI*	9050	42 30 20.97	288 26 28.71	193	N.A.
			42 30 20.51	288 26 29.79	138	C-5
I	COLDLK*	9424	54 44 38.02	249 57 25.85	597	N.A.
			54 44 37.26	249 57 21.90	548	C-5
I	EDWAFB*	9425	34 57 50.68	242 05 11.39	784	N.A.
			34 57 50.17	242 05 07.80	754	C-5
I	RIGLAT*	9428	56 56 54.00	24 03 42.00	5	European
			56 56 52.37	24 03 37.49	-15	C-5
I	POTDAM*	9429	52 22 55.00	13 04 01.00	111	European
			52 22 52.33	13 03 55.80	106	C-5
I	ZVENIG*	9430	55 41 37.70	36 46 03.00	145	European
			55 41 36.17	36 46 00.17	114	C-5

*These SAO station positions were derived by using the weighting scheme described in Reference 2, Section 2.

Table D3

STADAN Optical Source B.*

Name	Station No.	Latitude	Longitude	Geodetic Height (meters)	Datum
1BPOIN	1021	38°25'49!63	282°54'48!23	5	N.A.
		38 25 49.44	282 54 48.65	-50	C-5
1FTMYR	1022	26 32 51.89	278 08 03.93	19	N.A.
		26 32 53.08	278 08 03.80	-42	C-5
1OOMER	1024	-31 23 30.07	136 52 11.05	152	Australian
		-31 23 26.96	136 52 14.25	148	C-5
1QUITO	1025	-0 37 28.00	281 25 14.81	3649	N.A.
		-0 37 22.63	281 25 15.23	3554	C-5
1LIMAP	1026	-11 46 44.43	282 50 58.23	155	N.A.
		-11 46 37.56	282 50 58.86	34	C-5
1SATAG	1028	-33 09 07.66	289 19 51.35	922	N.A.
		-33 08 58.76	289 19 52.59	705	C-5
1MOJAV	1030	35 19 48.09	243 06 02.73	905	N.A.
		35 19 47.57	243 05 59.18	874	C-5
1JOBUR	1031	-25 52 58.86	27 42 27.93	1530	ARC (Cape)
		-25 53 02.70	27 42 25.41	1546	C-5
1NEWFL	1032	47 44 29.74	307 16 43.37	104	N.A.
		47 44 28.73	307 16 46.67	58	C-5
1COLEG	1033	64 52 19.72	212 09 47.17	162	N.A.
		64 52 17.78	212 09 37.29	139	C-5
1GFORK	1034	48 01 21.40	262 59 21.56	253	N.A.
		48 01 20.81	262 59 19.55	200	C-5
1WNKFL	1035	51 26 44.12	359 18 14.62	62	European
		51 26 40.67	359 18 08.35	76	C-5
1ROSMA	1042	35 12 06.93	277 07 41.01	914	N.A.
		35 12 07.03	277 07 40.81	857	C-5
1TANAN	1043	-19 00 27.09	47 18 00.46	1377	Tananarive
		-19 00 33.26	47 17 58.89	1355	C-5

*The coordinates in the above table are identical to the corresponding Minitrack site coordinates if they exist since the STADAN MOTS Cameras are collocated with the center of the Minitrack antenna array for calibration purposes.

Table D4

STADAN R/$\dot{R}$ Source B.

Name	Station No.	Latitude	Longitude	Geodetic Height (meters)	Datum
CARVON	1152	-24°54'14!85	113°42'55!05	38	Australian
		-24 54 12.29	113 42 58.54	10	C-5
ROSRAN	1126	35 11 45.05	277 07 26.23	880	N.A.
		35 11 45.15	277 07 26.02	823	C-5
MADGAR	1122	-19 01 13.32	47 18 09.45	1403	Tananarive
		-19 01 19.41	47 18 07.96	1382	C-5

Table D5

Navy Tranet Doppler Source C.

Name	Station No.	Latitude	Longitude	Geodetic Height (meters)	Datum
LASHAM	2006	51°11'10.62	358°58'30.51	182	European
		51 11 07.12	358 58 24.25	196	C-5
SANHES	2008	-23 13 01.74	314 07 50.59	608*	Correga Alegre
		-23 13 01.74	314 07 50.59	608	C-5
PHILIP	2011	14 58 57.79	120 04 25.98	8	Tokyo
		14 59 16.42	120 04 21.61	-70	C-5
SMTHFD	2012	-34 40 31.31	138 39 12.39	39	Australian
		-34 40 28.16	138 39 15.66	31	C-5
MISAWA	2013	40 43 04.63	141 20 04.69	-10	Tokyo
		40 43 14.63	141 19 51.45	38	C-5
ANCHOR	2014	61 17 01.98	210 10 37.46	61	N.A.
		61 16 59.60	210 10 28.60	44	C-5
TAFUNA	2017	-14 19 50.19	189 17 13.96	6*	USGS 1962 Astro
		-14 19 50.19	189 17 13.96	6	C-5
THULEG	2018	76 32 18.62	291 13 46.72	43	N.A.
		76 32 20.72	291 13 51.07	-7	C-5
MCMRDO	2019	-77 50 51.00	166 40 25.00	-43	Mercury
		-77 50 50.58	166 40 35.02	-29	C-5
WAHIWA	2100	21 31 26.86	202 00 00.63	380	Old Hawaiian
		21 31 14.95	202 00 09.83	368	C-5
LACRES	2103	32 16 43.75	253 14 48.25	1201	N.A.
		32 16 43.91	253 14 45.34	1162	C-5
LASHM2	2106	51 11 12.32	358 58 30.21	187	European
		51 11 08.82	358 58 23.95	201	C-5
APLMND	2111	39 09 47.83	283 06 11.07	146	N.A.
		39 09 47.60	283 06 11.52	90	C-5
PRETOR	2115	-25 56 46.09	28 20 53.00	1417	European
		-25 56 49.97	28 20 50.67	1595	C-5
SHEMYA	2739	52 43 01.52	174 06 51.43	44	N.A.
		52 42 56.52	174 06 44.17	89	C-5
BELTSV	2742	39 01 39.46	283 10 27.25	50	N.A.
		39 01 39.23	283 10 27.72	-5	C-5
STNVIL	2745	33 25 31.57	269 09 10.70	44	N.A.
		33 25 31.76	269 09 09.66	-10	C-5

*MSL

Table D6

Air Force Optical Source I.

Source	Name	Station No.	Latitude	Longitude	Geodetic Height (meters)	Datum
	ANTIGA	3106	17°08'51.68	298°12'37.41	7	N.A.
			17 08 53.88	298 12 39.19	-42	C-5
E	GRNVLE	3333	33 28 48.97	268 59 49.17	45	N.A.
			33 28 49.15	268 59 48.12	-9	C-5
	GRVILL	3334	33 25 31.95	269 05 11.35	42	N.A.
			33 25 32.14	269 05 10.30	-10	C-5
	USAFAC	3400	39 00 22.44	255 07 01.01	2191	N.A.
			39 00 21.99	255 06 58.32	2147	C-5
E	BEDFRD	3401	42 27 17.53	288 43 35.03	88	N.A.
			42 27 17.06	288 43 36.14	33	C-5
E	SEMMES	3402	30 46 49.35	271 44 52.37	79	N.A.
			30 46 49.85	271 44 51.64	23	C-5
	SWANIS	3404	17 24 16.57	276 03 29.87	83	N.A.
			17 24 18.90	276 03 29.71	18	C-5
	GRDTRK	3405	21 25 47.05	288 51 14.03	7	N.A.
			21 25 48.69	288 51 15.03	-48	C-5
	CURACO	3406	12 05 22.11	291 09 43.76	23	N.A.
			12 05 25.49	291 09 45.16	-34	C-5
	TRNDAD	3407	10 44 32.78	298 23 23.67	269	N.A.
			10 44 36.16	298 23 25.43	210	C-5
	TWINOK	3452	36 07 25.69	262 47 04.48	312	N.A.
			36 07 25.58	262 47 02.68	262	C-5
	ROTHGR	3453	51 25 00.00	9 30 06.00	351	European
			51 24 57.05	9 30 00.58	352	C-5
	ATHNGR	3463	37 53 30.00	23 44 30.00	16	European
			37 53 26.07	23 44 26.73	23	C-5
	TORRSP	3464	40 29 18.53	356 34 41.24	588	European
			40 29 14.10	356 34 36.06	635	C-5
	CHOFUJ	3465	35 39 57.00	139 32 12.00	49	Tokyo
			35 40 08.96	139 32 00.19	75	C-5
E	HUNTER	3648	32 00 05.87	278 50 46.36	17	N.A.
			32 00 06.32	278 50 46.32	-40	C-5
	JUPRAF	3649	27 01 14.80	279 53 13.72	26	N.A.
			27 01 16.02	279 53 13.72	-37	C-5
E	ABERDN	3657	39 28 18.97	283 55 44.56	4	N.A.
			39 28 18.71	283 55 45.10	-51	C-5
E	HOMEST	3861	25 30 24.69	279 36 42.69	18	N.A.
			25 30 26.02	279 36 42.70	-44	C-5
	CHYWYN	3902	41 07 59.20	255 08 02.65	1890	N.A.
			41 07 58.61	255 07 59.94	1845	C-5

Table D7

Army Map Service SECOR Source H.

Source	Name	Station No.	Latitude	Longitude	Geodetic Height (meters)	Datum
G	HERNDN	5001	38°59'37.69	282°40'16.68	119	N.A.
			38 59 37.47	282 40 17.08	64	C-5
I	CUBCAL	5200	32 48 00.00	242 52 00.00	101	N.A.
			32 47 59.74	242 51 56.55	71	C-5
I	LARSON	5201	47 11 00.00	240 40 00.00	354	N.A.
			47 10 58.76	240 39 55.68	319	C-5
I	WRGTON	5202	43 39 00.00	264 25 00.00	481	N.A.
			43 38 59.49	264 24 58.27	428	C-5
G	GREENV	5333	33 25 32.34	269 05 10.78	43	N.A.
			33 25 32.53	269 05 09.73	-10	C-5
	TRUKIS	5401	7 27 39.30	151 50 31.28	5*	Navy Iben Astro 1947
			7 27 39.30	151 50 31.28	5	C-5
	SWALLO	5402	-10 18 21.42	166 17 56.79	9*	1966 SECOR Astro
			-10 18 21.42	166 17 56.79	9	C-5
	KUSAIE	5403	5 17 44.43	163 01 29.88	7*	Astro 1962, 65, Allen Sodano Lt
			5 17 44.43	163 01 29.88	7	C-5
	GIZZOO	5404	-8 05 40.58	156 49 24.82	49*	Provisional DOS
			-8 05 40.58	156 49 24.82	49	C-5
	TARAWA	5405	1 21 42.13	172 55 47.26	7*	1966 SECOR Astro
			1 21 42.13	172 55 47.26	7	C-5
	NANDIS	5406	-17 45 31.01	177 27 02.83	17*	Viti Levu 1916
			-17 45 31.01	177 27 02.83	17	C-5
	CANTON	5407	-2 46 28.90	188 16 43.47	6*	1966 Canton Astro
			-2 46 28.90	188 16 43.47	6	C-5
	JONSTN	5408	16 43 51.68	190 28 41.55	6*	Johnston Island 1961
			16 43 51.68	190 28 41.55	6	C-5
	MIDWAY	5410	28 12 32.06	182 37 49.53	6	Midway Astro 1961
			28 12 29.60	182 37 49.53	6	C-5
	MAUIHI	5411	20 49 37.00	203 31 52.77	32	Old Hawaiian
			20 49 25.14	203 32 01.88	31	C-5
G	FTWART	5648	31 55 18.41	278 26 00.26	29	N.A.
			31 55 18.86	278 26 00.18	-27	C-5
G	HNTAFB	5649	32 00 04.04	278 50 43.17	27	N.A.
			32 00 04.49	278 50 43.13	-30	C-5
G	HOMEFL	5861	25 29 21.18	279 37 39.35	18	N.A.
			25 29 22.51	279 37 39.37	-44	C-5

*MSL

Table D8

USC&GS Optical Source F.

Name	Station No.	Latitude	Longitude	Geodetic Height (meters)	Datum
BELTVL	6002	39°01'39.03	283°10'26.94	45	N.A.
		39 01 38.80	283 10 27.40	-10	C-5
ASTRMD	6100	39 01 39.72	283 10 27.83	45	N.A.
		39 01 39.49	283 10 28.29	-10	C-5
TIMINS	6113	48 33 56.17	278 37 44.54	290	N.A.
		48 33 55.70	278 37 44.94	232	C-5

Table D9

SPEOPT Optical Source B.

Name	Station No.	Latitude	Longitude	Geodetic Height (meters)	Datum
1UNDAK	7034	48°01'21.40	262°59'21.56	255	N.A.
		48 01 20.81	262 59 19.55	201	C-5
1EDINB	7036	26 22 45.44	261 40 09.03	67	N.A.
		26 22 46.35	261 40 07.34	15	C-5
1COLBA	7037	38 53 36.07	267 47 42.12	271	N.A.
		38 53 35.81	267 47 40.85	218	C-5
1BERMD	7039	32 21 48.83	295 20 32.56	21	N.A.
		32 21 48.94	295 20 34.18	-28	C-5
1PURIO	7040	18 15 26.22	294 00 22.17	58	N.A.
		18 15 28.30	294 00 23.63	5	C-5
1GSFCP	7043	39 01 15.01	283 10 19.93	54	N.A.
		39 01 14.78	283 10 20.39	-1	C-5
1CKVLE	7044	38 22 12.50	274 21 16.81	187	N.A.
		38 22 12.33	274 21 16.28	131	C-5
1DENVR	7045	39 38 48.03	255 23 41.19	1796	N.A.
		39 38 47.54	255 23 38.52	1751	C-5
1JUM24	7071	27 01 12.77	279 53 12.31	25	N.A.
		27 01 14.00	279 53 12.30	-38	C-5
1JUM40	7072	27 01 13.17	279 53 12.49	25	N.A.
		27 01 14.39	279 53 12.49	-38	C-5
1JUPC1	7073	27 01 13.11	279 53 12.72	22	N.A.
		27 01 14.33	279 53 12.72	-41	C-5
1JUBC4	7074	27 01 13.33	279 53 12.76	25	N.A.
		27 01 14.55	279 53 12.76	-38	C-5
1SUDBR	7075	46 27 20.99	279 03 10.35	281	N.A.
		46 27 20.52	279 03 10.35	224	C-5
1JAMAC	7076	18 04 31.98	283 11 26.52	485	N.A.
		18 04 34.20	283 11 27.03	423	C-5

Table D10

SPEOPT LASER Source B.

Name	Station No.	Latitude	Longitude	Geodetic Height (meters)	Datum
ROSLAS	7051	35°11'46.60	277°07'26.23	879	N.A.
		35 11 46.70	277 07 26.02	822	C-5
GODLAS	7050	39 01 13.68	283 10 18.05	55	N.A.
		39 01 13.45	283 10 18.51	0	C-5

Table D11

International Optical Source I.

Source	Name	Station No.	Latitude	Longitude	Geodetic Height (meters)	Datum
	DELFTH	8009	52°00'09.24	4°22'21.23	23	European
			52 00 06.12	4 22 15.30	28	C-5
	MALVRN	8011	52 08 39.12	358 01 59.49	111	European
			52 08 35.68	358 01 53.03	125	C-5
D	ZIMWLD	8010	46 52 41.77	7 27 57.56	898	BERNE
			46 52 36.73	7 27 52.54	907	C-5

Table D12

SAO Optical.

Name	Station No.	Location
1ORGAN	9001	Organ Pass, New Mexico
1OLFAN	9002	Olifantsfontien, South Africa
1OOMER	9003	Woomera, Australia
1SPAIN	9004	San Fernando, Spain
1TOKYO	9005	Tokyo, Japan
1NATOL	9006	Naini Tal, India
1QUIPA	9007	Arequipa, Peru
1SHRAZ	9008	Shiraz, Iran
1CURAC	9009	Curacao, Lesser Antilles
1JUPTR	9010	Jupiter, Florida
1VILDO	9011	Villa Dolores, Argentina
1MAUIO	9012	Maui, Hawaii
OSLONR	9426	Oslo, Norway
AUSBAK	9023	Woomera, Australia
NATALB	9029	Natal, Brazil
AGASSI	9050	Cambridge, Massachusetts
COLDLK	9424	Cold Lake, Alberta
EDWAFB	9425	Edwards AFB, California
RIGLAT	9428	Riga, Latvia
POTDAM	9429	Potsdam, Germany
ZVENIG	9430	Zvenigorod, Russia

Table D13

STADAN Optical.

Name	Station No.	Location
1BPOIN	1021	Blossom Point, Maryland
1FTMYR	1022	Fort Myers, Florida
1OOMER	1024	Woomera, Australia
1QUITO	1025	Quito, Ecuador
1LIMAP	1026	Lima, Peru
1SATAG	1028	Santiago, Chile
1MOJAV	1030	Mojave, California
1JOBUR	1031	Johannesburg, Union of South Africa
1NEWFL	1032	St. John's, Newfoundland
1COLEG	1033	College, Alaska
1GFORK	1034	East Grand Forks, Minnesota
1WNKFL	1035	Winkfield, England
1ROSMA	1042	Rosman, North Carolina
1TANAN	1043	Tananarive, Madagascar

Table D14

STADAN R/Ṙ.

Name	Station No.	Location
CARVON	1152	Carnarvon, Australia
ROSRAN	1126	Rosman, North Carolina
MADGAR	1122	Tananarive, Madagascar

Table D15

Navy Tranet Doppler.

Name	Station No.	Location
LASHAM	2006	Lasham, England
SANHES	2008	Sao Jose dos Campos, Brazil
PHILIP	2011	San Miquel, Philippines
SMTHFD	2012	Smithfield, Australia
MISAWA	2013	Misawa, Japan
ANCHOR	2014	Anchorage, Alaska
TAFUNA	2017	Tafuna, American Samoa
THULEG	2018	Thule, Greenland
McMRDO	2019	McMurdo Sound, Antarctica
WAHIWA	2100	South Point, Hawaii
LACRES	2103	Las Cruces, New Mexico
LASHM2	2106	Lasham, England
APLMND	2111	APL Howard County, Maryland
PRETOR	2115	Pretoria, Union of South Africa
SHEMYA	2739	Shemya Island, Alaska
BELTSV	2742	Beltsville, Maryland
STNVIL	2745	Stoneville, Mississippi

Table D16

Air Force Optical.

Name	Station No.	Location
ANTIGA	3106	Antigua Island, Lesser Antilles
GRNVLE	3333	Stoneville, Mississippi
GRVILL	3334	Stoneville, Mississippi
USAFAC	3400	Colorado Springs, Colorado
BEDFRD	3401	L. G. Hanscom Field, Massachusetts
SEMMES	3402	Semmes Island, Georgia
SWANIS	3404	Swan Island, Caribbean Sea
GRDTRK	3405	Grand Turk, Caicos Islands
CURACO	3406	Curacao, Lesser Antilles
TRNDAD	3407	Trinidad Island
TWINOK	3452	Twin Oaks, Oklahoma
ROTHGR	3453	Rothwesten, West Germany
ATHNGR	3463	Athens, Greece
TORRSP	3464	Torrejon de Ardoz, Spain
CHOFUJ	3465	Chofu, Japan
HUNTER	3648	Hunter AFB, Georgia
JUPRAF	3649	Jupiter, Florida
ABERDN	3657	Aberdeen, Maryland
HOMEST	3861	Homestead AFB, Florida
CHYWYN	3902	Cheyenne, Wyoming

Table D17

Army Map Service SECOR.

Name	Station No.	Location
HERNDN	5001	Herndon, Virginia
CUBCAL	5200	San Diego, California
LARSON	5201	Moses Lake, Washington
WRGTON	5202	Worthington, Minnesota
GREENV	5333	Greenville, Mississippi
TRUKIS	5401	Truk Island, Caroline Islands
SWALLO	5402	Swallow Island, Santa Cruz Islands
KUSAIE	5403	Kusaie Islands, Caroline Island
GIZZOO	5404	Gizzoo, Gonzongo, Solomon Islands
TARAWA	5405	Tazawa, Gilbert Islands
NANDIS	5406	Nandi, Vitilevu, Fiji Islands
CANTON	5407	Canton Island, Phoenix Islands
JONSTN	5408	Johnston Island, Pacific Ocean
MIDWAY	5410	Eastern Island, Midway Islands
MAUIHI	5411	Maui, Hawaii
FTWART	5648	Fort Stewart, Georgia
HNTAFB	5649	Hunter AFB, Georgia
HOMEFL	5861	Homestead AFB, Florida

Table D18

USC&GS Optical.

Name	Station No.	Location
BELTVL	6002	Beltsville, Maryland
ASTRMD	6100	Beltsville, Maryland
TIMINS	6113	Timmins, Ontario

Table D19

SPEOPT Optical.

Name	Station No.	Location
1UNDAK	7034	Univ. North Dakota, Grand Forks, North Dakota
1EDINB	7036	Edinburg, Texas
1COLBA	7037	Columbia, Missouri
1BERMD	7039	Bermuda Island
1PURIO	7040	San Juan, Puerto Rico
1GSFCP	7043	GSFC, Greenbelt, Maryland
1CKVLE	7044	Clarksville, Indiana
1DENVR	7045	Denver, Colorado
1JUM24	7071	Jupiter, Florida
1JUM40	7072	Jupiter, Florida
1JUPC1	7073	Jupiter, Florida
1JUBC4	7074	Jupiter, Florida
1SUDBR	7075	Sudbury, Ontario
1JAMAC	7076	Jamaica, B. W. I.

Table D20

SPEOPT LASER.

Name	Station No.	Location
ROSLAS	7051	Rosman, North Carolina
GODLAS	7050	GSFC, Greenbelt, Maryland

Table D21

International Optical.

Name	Station No.	Location
DELFTH	8009	Delft, Holland
MALVRN	8011	Malvern, England
ZIMWLD	8010	Berne, Switzerland

References—Appendix D

1. Lundquist, C. A., Veis, G., "Geodetic Parameters for a 1966 Smithsonian Institution Standard Earth," Smithsonian Astrophysical Observatory Special Report 200, Vol. 1, 1966.

2. Lerch, F. J., Marsh, J. G., D'Aria, M. D., Brooks, R. L., "GEOS I Tracking Station Positions on the SAO Standard Earth (C-5)," GSFC Document X-552-68-70.

3. Lerch, F. J., Doll, C. E., Moss, S. J., O'Neill, B., "The Determination and Comparison of the GRARR MADGAR Site Location," GSFC Document X-552-67-540, October 1967.

Appendix E

TABLE OF GEOS-I ORBIT NUMBERS
FROM 12/31/65 TO 1/5/66

Table E1

Pass Numbers for GEOS-I.
(Mean Period of GEOS-I at epoch 12/31/65 $01^H\ 38^M\ 22^S$ = $2^H.005393$ = $120^M.3236$)

Pass No.	From			To		
650	12/31/65	01^H	18^M	12/31/65	03^H	17^M
651		03	18		05	17
652		05	18		07	18
653		07	19		09	18
654		09	19		11	18
655		11	19		13	18
656		13	19		15	19
657		15	20		17	19
658		17	20		19	19
659		19	20		21	20
660		21	21		23	20
661		23	21	01/01/66	01	20
662	01/01/66	01	21		03	21
663		03	22		05	21
664		05	22		07	21
665		07	22		09	21
666		09	22		11	22
667		11	23		13	22
668		13	23		15	22
669		15	23		17	23
670		17	24		19	23
671		19	24		21	23
672		21	24		23	24
673		23	25	01/02/66	01	24
674	01/02/66	01	25		03	24
675		03	25		05	24
676		05	25		07	25
677		07	26		09	25
678		09	26		11	26
679		11	26		13	26
680		13	27		15	26
681		15	27		17	26
682		17	27		19	27
683		19	28		21	27
684		21	28		23	27
685		23	28	01/03/66	01	28
686	01/03/66	01	29		03	28
687		03	29		05	28
688		05	29		07	28
689		07	29		09	29
690		09	30		11	29
691		11	30		13	29
692		13	30		15	30
693		15	31		17	30
694		17	31		19	30
695		19	31		21	31
696		21	32		23	31
697		23	32	01/04/66	01	31

Table E1 (continued)

Pass No.	From			To		
698	01/04/66	01^{H}	32^{M}	01/04/66	03^{H}	31^{M}
699		03	32		05	32
700		05	33		07	32
701		07	33		09	32
702		09	33		11	33
703		11	34		13	33
704		13	34		15	33
705		15	34		17	34
706		17	35		19	34
707		19	35		21	34
708		21	35		23	34
709		23	35	01/05/66	01	35
710	01/05/66	01	36		03	35
711		03	36		05	35
712		05	36		07	36